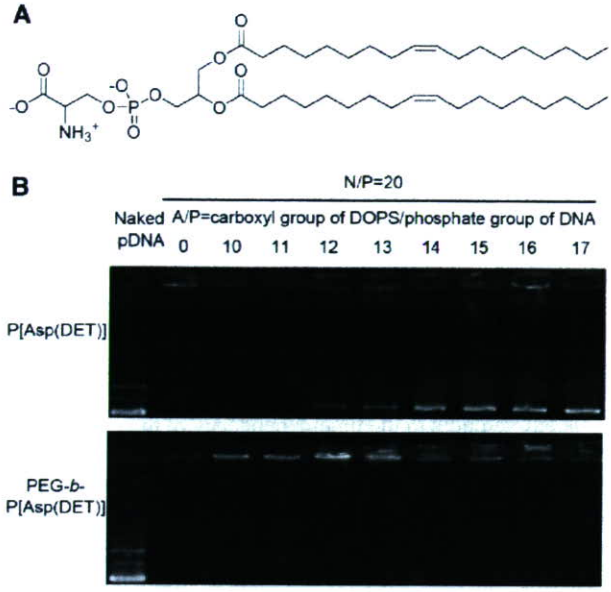

Fig. 7. Electrophoresis of P[Asp(DET)] polyplex and PEG-*b*-P[Asp(DET)] polyplex micelle. A) Chemical structure of anionic lipid (DOPS). B) Electrophoresis of P[Asp(DET)] polyplex and PEG-*b*-P[Asp(DET)] polyplex micelle solutions prepared at the *N*/*P* ratio of 20 after mixing with anionic lipid, DOPS at different *A*/*P* ratios.

cationic polymers and in some cases protected by biocompatible polymers to improve stability in biological media [9–12], prolonged evaluation of the gene expression might be necessary because it may take time for the decondensation and the release (the unpacking process) of pDNA from the polyplexes. Another important discrepancy between in vitro conventional monolayer cultures and in vivo tissues is the three-dimensional environments (e.g., cell–cell and cell–ECM interactions) for the cells. Thus, the three-dimensional features of in vivo tissues should be considered for in vitro evaluation of gene transfection. In this regard, three-dimensional multicellular spheroids (MCTS) might be a promising in vitro model for the evaluation of non-viral vectors worked under in vivo conditions.

In the transfection study using MCTS models, a long-term life span of MCTS might allow the prolonged evaluation of gene expression by non-viral vectors. Indeed, the spheroids transfected with the polyplexes showed the gene expression of fluorescent protein for over 10 days (Figs. 5 and 6). We also found that the small spheroids with diameters of ca 100 μm were more sensitive against the polyplex-induced cytotoxicity than monolayer cultured cells, while relatively large (ca 700 nm) MCTS did not show such high sensitivity to polyplex-induced toxicity (data not shown). It appears that the small spheroids may have a relatively weak structure due to their immature development of cell–cell and cell–ECM interactions. In contrast, the large spheroids have a heterogeneous structure consisting of outer layers of viable cells and a solid core of necrotic or hypoxic cells (Fig. 4C), resembling a monolayer cell culture where the cells adhere to the hard substrate. Such morphological differences between small and large spheroids may account for their different sensitivities against polyplex-induced cytotoxicity.

Among the evaluated polyplexes from the cationic homopolymers, P[Asp(DET)] polyplexes showed the most efficient transfection efficiency with the least cytotoxicity against monolayer cultured cells (Figs. 2 and 3). The efficient transfection by P[Asp(DET)] may be explained by their buffering capacity (Fig. 1A), which may facilitate the cytoplasmic delivery of the polyplexes through destabilization of the endosomal membrane by an increased ion osmotic pressure (proton sponge effect) [2]. However, P[Asp(DPT)] polyplexes at $N/P=10$ also showed an appreciably high transfection activity (Fig. 2A) regardless of the lack of proton buffering capacity (Fig. 1A), suggesting that the proton sponge effect may not fully explain the efficient gene transfection by P[Asp(DPT)] polyplex. Detailed mechanisms involved in the gene transfection process of P[Asp(DET)] and P[Asp(DPT)] polyplexes are under investigation in our laboratory and will be reported elsewhere in the near future. The cytotoxicity of P[Asp(DET)] polyplexes was remarkably low compared with other polyplexes from P[Asp(DPT)] or L/BPEI (Fig. 3). Also, the transfection study using MCTS models revealed that P[Asp(DET)] polyplexes at $N/P=10$ and 20 showed successful transfection with maintaining the MCTS structures, while the destruction of MCTS occurred by challenging L/BPEI and P[Asp(DPT)] polyplexes (Fig. 5B). The destruction of MCTS by the polyplexes (Fig. 5B) is in line with the cytotoxicity of the polyplexes against the monolayer cultured cells (Fig. 3), indicating the minimally cytotoxic nature of P[Asp(DET)] polyplexes. The unique molecular feature of a franking ethylenediamine unit, including a specific *gauche*-conformation of the mono-protonated form preferential at the physiological state, may have a role in this appreciably high biocompatibility of P[Asp(DET)] polyplexes. This hypothesis remains to be clarified yet.

PEGylation of polycations apparently improved the biocompatibility of polyplexes, as indicated by the stability of the MCTS structure after transfection. The PEG-*b*-P[Asp(DPT)] polyplex micelles at $N/P=10$ did not cause the destruction of the MCTS (Fig. 5C), whereas the destruction occurred through the transfection with P[Asp(DPT)] polyplexes at the same *N*/*P* ratio (Fig. 5B). Likewise, the PEG-*b*-P[Asp(DET)] polyplex micelles at $N/P=40$ showed no MCTS destruction, while the destruction of MCTS was observed in the transfection with the P[Asp(DET)] polyplexes at the same *N*/*P* ratio. Note that such a difference in biocompatibility between PEG-*b*-P[Asp(DET)] polyplex micelles and P[Asp(DET)] polyplexes could not be detected by the cytotoxicity study using the monolayer cultured cells, but was detected using the MCTS models. This result suggests that MCTS models are more sensitive than monolayer cultured cells to polyplex-induced toxicity, allowing them to detect the improved biocompatibility of the polyplex system through the PEGylation of polycations. Besides its positive effect of improving the cytotoxicity of the polyplexes, PEGylation of the polyplex changed the time-dependent profiles of the transfected gene expression. As seen in Fig. 6C, the relative intensity of the transfected fluorescent protein (i.e., *Venus*) in MCTS, which is defined as the total intensity divided by the volume of spheroids, followed significantly different time courses between P[Asp(DET)] polyplexes and PEG-*b*-P[Asp(DET)] polyplex micelles: the latter with relatively high *N*/*P* ratios, such as 20 and 40, had peak relative intensities at 4 days after transfection, while the former exhibited a continuous decrease in the relative

intensities with time (Fig. 6C). These results suggest that the polyplex micelles from PEG-*b*-polycation copolymers may be capable of delaying gene expression compared with polyplexes from cationic homopolymers. This is consistent with our previous report that in vivo gene expression of polyplex micelles in the liver revealed a delayed onset, and was observed 5 days after intravenous injection [13]. We hypothesized that such delayed gene expression from the polyplex micelles might be due to their higher stability or their delayed unpacking of pDNA in intracellular compartments. This may be supported from the increased tolerability of PEG-*b*-P[Asp(DET)] polyplex micelles compared to P[Asp(DET)] polyplexes against the pDNA exchange reaction with an anionic lipid, DOPS (Fig. 7). It is also consistent with our previous report that PEG-*b*-poly(L-lysine) polyplex micelles showed higher stability than poly(L-lysine) polyplexes in the thermal melting study of DNA [8]. The decrease in the local permittivity of the polyplex core, surrounded by PEG palisades and/or a steric protection of the polyplex core by PEG palisades, may contribute to the stabilization of polyplex micelles against the exchange reaction with anionic components in intracellular environments. It is worth noting that the time-dependency of gene expression differs between polyplex systems, which was clearly investigated through the prolonged observation of transfected cells in the form of spheroids.

In conclusion, we used MCTS models to study the effects of chemical structures and PEGylation of cationic poly(*N*-substituted asparagine) polyplexes on gene transfection, particularly focusing on both polyplex toxicity and the duration of gene expression. Through this evaluation, the feasible properties, i.e., biocompatibility and prolonged gene expression, of PEG-*b*-P[Asp(DET)] micelles were clarified, facilitating their utility for in vivo gene transfection as recently demonstrated in a rabbit carotid artery model [15]. Also, this study underscores the usefulness of MCTS models in screening non-viral vectors in conditions mimicking in vivo environments.

Acknowledgement

We are grateful to Mr. S. Fukushima and Mr. S. Asano for polymer synthesis. This work was supported by the Core Research for Evolutional Science and Technology (CREST), Japan Science and Technology Agency (JST), and the Health and Labor Sciences Research Grants in Research on Advanced Medical Technology in Nanomedicine Area from the Ministry of Health, Labor and Welfare (MHLW), Japan.

Appendix A. Supplementary data

Supplementary data associated with this article can be found, in the online version, at doi:10.1016/j.jconrel.2007.05.012.

References

[1] G.Y. Wu, C.H. Wu, Receptor-mediated in vitro gene transformation by a soluble DNA carrier system, J. Biol. Chem. 262 (1987) 4429–4432.
[2] O. Boussif, F. Lezoualc'h, M.A. Zanta, M.D. Mergny, D. Scherman, B. Demeneix, J.P. Behr, A versatile vector for gene and oligonucleotide transfer into cells in culture and in vivo: Polyethyleneimine, Proc. Natl. Acad. Sci. U. S. A. 92 (1995) 7297–7301.
[3] D.W. Pack, A. Hoffman, S. Pun, P.S. Stayton, Design and development of polymers for gene delivery, Nat. Rev. Drug. Discov. 4 (2005) 581–593.
[4] A.V. Kabanov, I.V. Astafieva, I.V. Maksimova, E.M. Lukanidin, G.P. Georgiev, V.A. Kabanov, Efficient transformation of mammalian cells using DNA interpolyelectrolyte complexes with carbon chain polycations, Bioconjug. Chem. 4 (1993) 448–454.
[5] M. Harada-Shiba, K. Yamauchi, A. Harada, I. Takamisawa, K. Shimokado, K. Kataoka, Polyion complex micelles as vectors in gene therapy — pharmacokinetics and in vivo gene transfer, Gene Ther. 9 (2002) 407–414.
[6] M. Ogris, E. Wagner, Targeting tumors with non-viral gene delivery systems, Drug Discov. Today 7 (2002) 479–485.
[7] K. Kataoka, G.S. Kwon, M. Yokoyama, T. Okano, Y. Sakurai, Block copolymer micelles as vehicles for drug delivery, J. Control. Release 24 (1993) 119–132.
[8] S. Katayose, K. Kataoka, Water-soluble polyion complex associates of DNA and poly(ethylene glycol)-poly(l-lysine) block copolymer, Bioconjug. Chem. 8 (1997) 702–707.
[9] M. Ogris, S. Brunner, S. Schüller, S. Kircheis, E. Wagner, PEGylated DNA/transferrin-PEI complexes: reduced interaction with blood components, extended circulation in blood and potential for systemic gene delivery, Gene Ther. 6 (1999) 595–605.
[10] T. Merdan, K. Kunath, H. Petersen, U. Bakowsky, K.H. Voigt, J. Kopecek, T. Kissel, PEGylation of poly(ethylene imine) affects stability of complexes with plasmid DNA under in vivo conditions in a dose-dependent manner after intravenous injection in to mice, Bioconjug. Chem. 16 (2005) 785–792.
[11] K. Itaka, A. Harada, K. Nakamura, H. Kawaguchi, K. Kataoka, Evaluation by fluorescence resonance energy transfer of the stability of nonviral gene delivery vectors under physiological conditions, Biomacromolecules 3 (2002) 841–845.
[12] K. Itaka, K. Yamauchi, A. Harada, K. Nakamura, H. Kawaguchi, K. Kataoka, Polyion complex micelles from plasmid DNA and poly(ethylene glycol)-poly (l-lysine) block copolymers as serum-tolerable polyplex system: physicochemical properties of micelles relevant to gene transfection efficiency, Biomaterials 24 (2003) 4495–4506.
[13] K. Miyata, Y. Kakizawa, N. Nishiyama, Y. Yamasaki, T. Watanabe, M. Kohara, K. Kataoka, Freeze-dried formulations for in vivo gene delivery of PEGylated polyplex micelles with disulfide crosslinked cores to the liver, J. Control. Release 109 (2005) 15–23.
[14] N. Kanayama, S. Fukushima, N. Nishiyama, K. Itaka, W.D. Jang, K. Miyata, Y. Yamasaki, U.I. Chung, K. Kataoka, A PEG-based biocompatible block catiomer with high buffering capacity for the construction of polyplex micelles showing efficient gene transfer toward primary cells, Chem. Med. Chem. 1 (2006) 439–444.
[15] D. Akagi, M. Oba, H. Koyama, N. Nishiyama, S. Fukushima, T. Miyata, H. Nagawa, K. Kataoka, Biocompatible micellar nanovectors achieve efficient gene transfer to vascular lesions without cytotoxicity and thrombus formation. Gene Therapy, in press.
[16] R.M. Sutherland, Cell and environment interactions in tumor microregions: the multicell spheroid model, Science 240 (1988) 177–184.
[17] H.R. Mellor, L.A. Davies, H. Caspar, C.R. Pringle, S.C. Hyde, D.R. Gill, R. Callaghan, Optimising non-viral gene delivery in a tumour spheroid model, J. Gene Med. 8 (2006) 1160–1170.
[18] H. Niwa, K. Yamamura, J. Miyazaki, Efficient selection for high-expression transfectants with a novel eukaryotic vector, Gene 108 (1991) 193–199.
[19] T. Nagai, K. Ibata, E.S. Park, M. Kubota, K. Mikoshiba, A. Miyawaki, A variant of yellow fluorescent protein with fast and efficient mutation for cell-biological application, Nat. Biotechnol. 20 (2002) 87–90.
[20] G.P. Tang, J.M. Zeng, S.J. Gao, Y.X. Ma, L. Shi, Y. Li, H.P. Too, S. Wang, Polyethylene glycol modified polyethylenimine for improved CNS gene transfer, Biomaterials 24 (2003) 2351–2362.
[21] M. Haji-Karim, J. Carlsson, Proliferation and viability in cellular spheroids of human origin, Cancer Res. 38 (1978) 1457–1464.
[22] L.A. Kunz-Schughart, Multicellular tumor spheroids; intermediates between monolayer culture and in vivo tumor, Cell Biol. Int. 23 (1999) 157–161.

VOLUME 121 NO. 3, 28 AUGUST 2007 ISSN: 0168-3659

journal of controlled release

OFFICIAL JOURNAL OF THE CONTROLLED RELEASE SOCIETY
AND THE JAPANESE SOCIETY OF DRUG DELIVERY SYSTEM

Available online at www.sciencedirect.com
ScienceDirect
Journal of Controlled Release 121 (2007) 146–155
journal of controlled release
www.elsevier.com/locate/jconrel

Optimization of (1,2-diamino-cyclohexane)platinum(II)-loaded polymeric micelles directed to improved tumor targeting and enhanced antitumor activity

Horacio Cabral [a], Nobuhiro Nishiyama [b], Kazunori Kataoka [a,b,c,*]

[a] *Department of Materials Engineering, Graduate School of Engineering, The University of Tokyo, 7-3-1 Hongo, Bunkyo-ku, Tokyo 113-8656, Japan*
[b] *Center for Disease Biology and Integrative Medicine, Graduate School of Medicine, The University of Tokyo, 7-3-1 Hongo, Bunkyo-ku, Tokyo 113-0033, Japan*
[c] *Center for NanoBio Integration, The University of Tokyo, 7-3-1 Hongo, Bunkyo-ku, Tokyo, 113-8656, Japan*

Received 19 March 2007; accepted 21 May 2007
Available online 29 May 2007

Abstract

Polymeric micelles are promising nanocarriers, which might enhance the efficacy of antitumor drugs. Herein, polymeric micelles incorporating dichloro(1,2-diamino-cyclohexane)platinum(II) (DACHPt), the oxaliplatin parent complex, were prepared through the polymer-metal complex formation of DACHPt with poly(ethylene glycol)-*b*-poly(glutamic acid) [PEG-*b*-P(Glu)] block copolymer having different lengths of the poly (glutamic acid) block [p(Glu): 20, 40, and 70 U]. The resulting micelles were studied with the aim of optimizing the system's biological performance. DACHPt-loaded micelles (DACHPt/m) were approximately 40 nm in diameter and had a narrow size distribution. *In vivo* biodistribution and antitumor activity experiments (CDF_1 mice bearing the murine colon adenocarcinoma C-26 inoculated subcutaneously) showed 20-fold greater accumulation of DACHPt/m at the tumor site than free oxaliplatin to achieve substantially higher antitumor efficacy. Moreover, the micelles prepared from PEG-*b*-P(Glu) with 20 U of P(Glu) exhibited the lowest non-specific accumulation in the liver and spleen to critically reduce non-specific accumulation, resulting in higher specificity to solid tumors. The antitumor effect of DACHPt/m was also evaluated on multiple metastases generated from intraperitoneally injected bioluminescent HeLa (HeLa-Luc) cells. The *in vivo* bioluminescent data indicated that DACHPt/m decreased the signal 10-to 50-fold compared to the control indicating a very strong antitumor activity. These results suggest that DACHPt/m could be an outstanding drug delivery system for oxaliplatin in the treatment of solid tumors.

Keywords: Polymeric micelles; DACHPt; Oxaliplatin; Biodistribution; Antitumor activity

1. Introduction

Oxaliplatin, oxalato(trans-*l*-1,2-diaminocyclohexane)platinum(II), is a third-generation platinum drug approved by the United States Food and Drug Administration in 2004 for the first-line treatment of advanced colorectal cancer in combination with 5-fluorouracil/folinic acid (5-FU/LV) [1]. The incorporation of oxaliplatin into the colorectal cancer program represents a major improvement in the treatment of the disease. The synergistic effects between oxaliplatin and 5-FU/LV significantly increased the response rates, improved the time-sensitive response parameters, and contributed to the removal of heretofore unresectable hepatic metastases, thereby changing the natural history of the malignancy. Nevertheless, oxaliplatin distributes rapidly to the whole body and, even though it shows better tolerability relative to other platinum drugs, cumulative peripheral distal neurotoxicity and acute dysesthesias restrain the range of working doses [2,3]. Consequently, enormous effort has been dedicated to develop drug delivery systems that increase the blood residence time of oxaliplatin and other platinum drugs, and target those drugs to solid tumors by taking advantage of the enhanced permeability and retention (EPR) effect [4]. Liposomes and macromolecular carriers (water soluble polymer–drug conjugates) have been the first attempts

* Corresponding author. Department of Materials Engineering, Graduate School of Engineering, The University of Tokyo, 7-3-1 Hongo, Bunkyo-ku, Tokyo 113-8656, Japan. Tel.: +81 3 5841 7138; fax: +81 3 5841 7139.
E-mail address: kataoka@bmw.t.u-tokyo.ac.jp (K. Kataoka).

0168-3659/$ - see front matter © 2007 Elsevier B.V. All rights reserved.
doi:10.1016/j.jconrel.2007.05.024

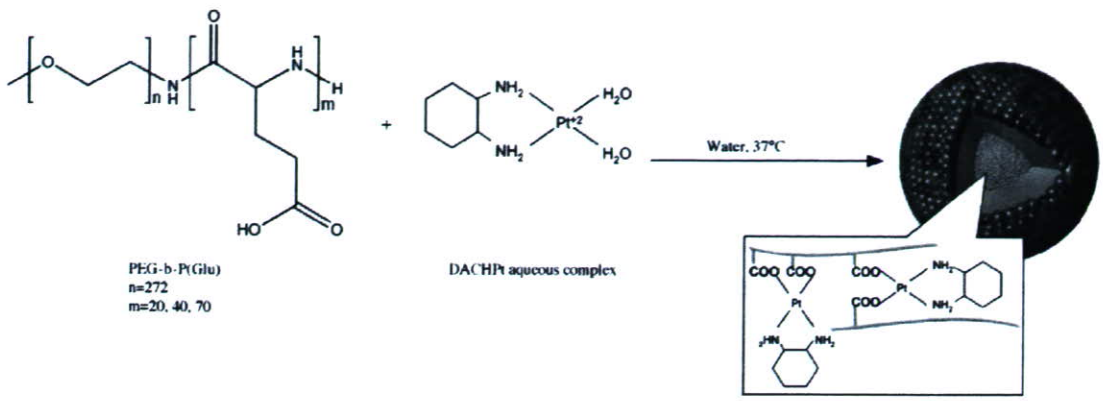

Fig. 1. Formation of DACHPt-loaded micelle (DACHPt/m).

to be considered [5–11]. However, successful formulations have not been developed yet due to unfavorable properties of platinum drugs. For example, the low water solubility of platinum drugs limits their loading efficacy into liposomal formulations (only 1 to 7% of drug loading). Moreover, liposomes incorporating the drug in the lipid bilayer showed rapid leakage of the drugs during storage and in the bloodstream [6]. In the case of macromolecular-drug formulations at high substitution ratios, they show reduced solubility due to the enlarged cohesive forces and to the cross-linking formation between polymer chains [8].

A novel approach to the design of nanocarriers for platinum drugs has been utilizing polymeric micelles [12–15]. Polymeric micelles present unique advantages over other types of drug-carrier systems: (i) prolonged blood circulation due to the efficient stealthy behavior of the dense shell of poly(ethylene glycol) (PEG), which hinders the adsorption of plasma proteins on the surface of the nanostructure and avoids recognition by the reticuloendothelial system (RES); (ii) easiness in encapsulating different compounds by modulating the micelle-forming block copolymers; (iii) reduced cumulative toxicity because of the micellar self-dissociation into unimers with molecular weight lower than that of the threshold of glomerular excretion; (iv) simplicity in size control by changing the chemical composition of block copolymers; (v) deeper tumor penetration due to the sub-100 nm size; (vi) facile management of the drug release in a controlled and environment-sensitive manner by modification of the drug-polymer system; and (vii) improved targeting capability by conjugating pilot molecules on the surface of micelles.

The first generation of platinum-drug-loaded micelles was prepared by the metal-complex formation between cis-dichlorodiammineplatinum(II) (cisplatin, CDDP) and poly(ethylene glycol)-*b*-poly(amino acid) block copolymers [16–21]. The exceptional physicochemical and biological properties of the CDDP-loaded micelle indicate them as an outstanding delivery system for CDDP complexes and a phase I clinical trial is being performed in United Kingdom (NC-6004, Nanocarrier, Japan). More recently, new platinum-drug-loaded polymeric micelles incorporating the oxaliplatin active complex were prepared by the complexation of dichloro(1,2-diaminocyclohexane)platinum(II) (DACHPt) with PEG-*b*-P(Glu) [22]. Previous studies demonstrated that the DACHPt-loaded micelle (DACHPt/m) might maintain its micellar structure for approximately 10 days in 10 mM PBS plus 150 mM NaCl, considerably longer than the stability of the CDDP-loaded micelles (ca 50 h) under the same conditions, while the drug was released from the micelle core in a sustained manner. Moreover, DACHPt/m showed remarkably prolonged blood circulation and more than 20-fold greater accumulation in tumor tissue compared to free oxaliplatin. According to these results, DACHPt/m seems to be an exceptionally promising carrier for the active complexes of oxaliplatin.

Herein, the *in vitro* and *in vivo* biological properties of DACHPt/m prepared with poly(ethylene glycol)-*b*-poly(glutamic acid) [PEG-*b*-P(Glu)] were studied with the aim of optimizing the biological performance of the micelle. Thus, PEG-*b*-P(Glu) having different P(Glu) block lengths (20, 40, and 70 U) were synthesized and used for the micelle preparation. DACHPt/m was phisicochemically characterized to determine the size, size distribution, zeta-potential, drug loading, and weight fraction of block copolymer. The *in vivo* behavior of DACHPt/m was assessed by the biodistribution and antitumor activity experiments using CDF_1 mice bearing the murine colon adenocarcinoma 26 (C-26). Although oxaliplatin had shown low efficacy against this tumor model [23], we found that DACHPt/m considerably increased the antitumor activity of the drug, probably by maintaining high drug levels within the tumor for a prolonged period. Furthermore, since chemotherapy is used in patients with metastatic disease and all the established therapies reveal poor efficiency at the late stage of the disease [24], new therapeutic strategies are urgently needed. Moreover, given that the very low prognosis of late-stage cervical carcinoma [25] (5 years after treatment 15% or fewer of women with stage IV cancer survive) is mainly due to metastasis to the abdomen or the lungs, the antitumor activity of DACHPt/m was evaluated against a bioluminescent intraperitoneal metastatic tumor model of cervical cancer.

2. Experimental

2.1. Materials

γ-benzyl L-glutamate was purchased from Sigma Chemical (St. Louis, MO). Bis(trichloromethyl)carbonate (triphosgene) was purchased from Tokyo Kasei Kogyo (Tokyo, Japan). *N,N-*

Table 1
DACHPt-loaded micelles (DACHPt/m) size, zeta-potential and drug loading

Micelle formulation	Size(nm)	Zeta-potential(mV)	Drug loading, [DACHPt]/[Glu]
DACHPt/m 12–20	37	−3	0.317
DACHPt/m 12–40	40	−4	0.323
DACHPt/m 12–70	41	−4	0.288

dimethylformamide (DMF) and 3-(4,5-dimethylthiazol-2-yl)-2,5-diphenyltetrazolium bromide (MTT) were obtained from Wako Pure Chemical (Osaka, Japan). Dichloro(1,2-diamminocyclohexane)platinum(II) (DACHPt) and $AgNO_3$ were purchased from Aldrich Chemical (Milwaukee, WI). α-methoxy-ω-aminopoly(ethylene glycol) (CH_3O–PEG–NH_2; Mw= 12,000) was purchased from Nippon Oil and Fats (Tokyo, Japan).

2.2. Cell lines and animals

Murine colon adenocarcinoma 26 (C-26) cells were kindly supplied by the National Cancer Center (Tokyo, Japan). C-26 cells were maintained in RPMI 1640 medium (Sigma Chemical) containing 10% fetal bovine serum in a humidified atmosphere containing 5% CO_2 at 37 °C. Bioluminescent HeLa (HeLa-Luc) cells were purchased from Xenogen (Alameda, CA). Luciferase stable-HeLa-Luc cells were maintained in Dulbecco's Modified Eagle Medium (Sigma Chemical Co., Inc.) containing 10% fetal bovine serum in a humidified atmosphere containing 5% CO_2 at 37 °C for no more than two weeks to assure luciferase luminescence stability.

Table 2
Accumulation ratios and area under the curve (AUC) ratios between tumor and normal organs at 48 h after administration of DACHPt-loaded micelles (DACHPt/m)[a] prepared with PEG-*b*-P(Glu) 12–40 and free oxaliplatin

Drug	Accumulation ratio				AUC ratio[b]	
	Tumor/ liver	Tumor/ spleen	Tumor/ kidney	Tumor/ liver	Tumor/ spleen	Tumor/ kidney
DACHPt/m 12–40	1.25	1.26	3.9	1.25	1.53	3.12
Oxaliplatin	0.9	0.18	0.42	1.1	0.32	0.9

[a] Dose: 0.1 mg per mouse on Pt basis.
[b] AUC calculated by trapezoidal rule up to 48 h.

Severe Combined Immunodeficiency (SCID) and CDF_1 mice (female; 18–20 g body weight; 6 weeks old) were purchased from Charles River Japan (Kanagawa, Japan). All animal experiments were carried out in accordance with the Guide for the Care and Use of Laboratory Animals as stated by the NIH. Sterile procedures were followed to assure that SCID mice were disease-free.

2.3. Preparation of PEG-b-P(Glu)

PEG-*b*-P(Glu) block copolymers were synthesized in accordance with the previously described synthetic method

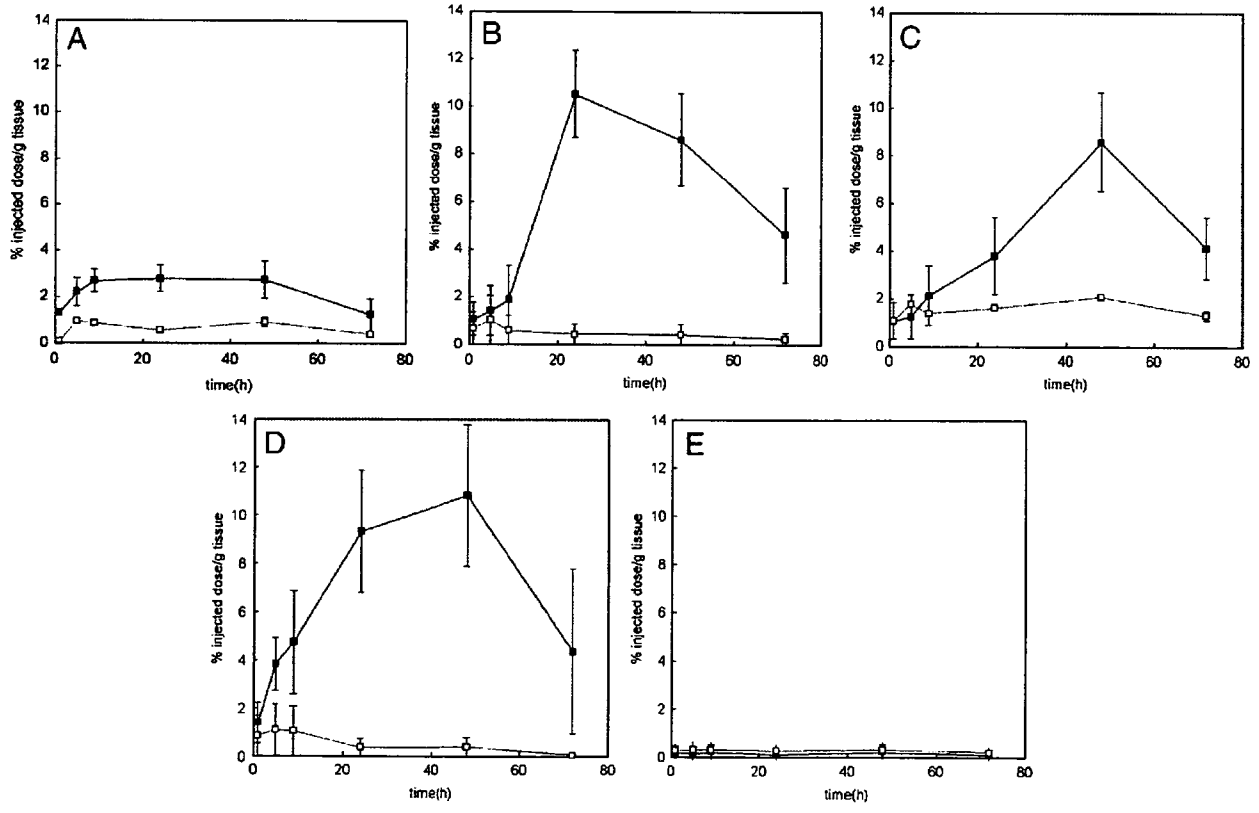

Fig. 2. Biodistribution of oxaliplatin (□) and DACHPt-loaded micelle (DACHPt/m) prepared with PEG-*b*-P(Glu) 12–40 (■): A. Kidney; B. Liver; C. Spleen; D. Tumor; E. Muscle. Data are expressed as averages±S.D.

[20] with a minor modification. Briefly, the *N*-carboxy anhydride of γ-benzyl L-glutamate was synthesized by the Fuchs–Farthing method using triphosgene. Then, *N*-carboxy anhydride of γ-benzyl L-glutamate was polymerized in DMF, initiated by the primary amino group of CH_3O–PEG–NH_2, to obtain PEG-*b*-poly(γ-benzyl L-glutamate) (PEG-*b*-PBLG) block copolymer with different PBLG block lengths (20, 40, and 70 U). The molecular weight distribution of PEG-*b*-PBLG was determined by gel permeation chromatography [column: TSK-gel $G3000_{HHR}$, $G4000_{HHR}$ (Tosoh, Yamaguchi, Japan); eluent: DMF containing 10 mM LiCl; flow rate: 0.8 ml/min; detector: refractive index (RI); temperature: 25 °C]. The polymerization degree of PBLG was verified by comparing the proton ratios of methylene units in PEG (–OCH_2CH_2–: δ=3.7 ppm) and phenyl groups of PBLG (–$CH_2C_6H_5$: δ=7.3 ppm) in ^{1}H-NMR measurement [JEOL EX270 (JEOL, Tokyo, Japan); solvent: DMSO-d_6; temperature: 80 °C]. PEG-*b*-PBLG was deprotected by mixing with 0.5 N NaOH at room temperature to obtain PEG-*b*-P(Glu). Complete deprotection was confirmed by ^{1}H-NMR measurement (solvent: D_2O; temperature: 25 °C). The compositions of PEG-*b*-P(Glu) are abbreviated as PEG-*b*-P(Glu) 12–20, PEG-*b*-P(Glu) 12–40 and PEG-*b*-P(Glu) 12–70 for the different P(Glu) block lengths (20, 40, and 70 U, respectively).

2.4. Preparation of DACHPt-loaded micelles (DACHPt/m)

DACHPt/m were prepared according to a previously described method [22]. Briefly, DACHPt (5 mM) was suspended in distilled water and mixed with silver nitrate ([$AgNO_3$]/[DACHPt]=1) to form an aqueous complex. The solution was kept in the dark at 25 °C for 24 h. AgCl precipitates found after the reaction were eliminated by centrifugation. Afterward, the supernatant was purified by passage through a 0.22 μm filter. Then, PEG-*b*-P(Glu) 12–20, 12–40, or 12–70 ([Glu]=5 mmol/liter) was added to DACHPt aqueous complex solution ([DACHPt]/[Glu]=1.0) and reacted for 120 h to prepare DACHPt/m. The prepared micelles were purified by ultrafiltration [molecular weight cutoff size (MWCO): 100,000]. The size distribution of DACHPt/m was evaluated by the dynamic light scattering (DLS) measurement at 25 °C using a Photal DLS-7000 dynamic laser scattering spectrometer (Otsuka Electronics, Osaka, Japan). The zeta-potential of DACHPt/m was determined using a Zetasizer Nano ZS90 (Malvern Instruments, Worcestershire, United Kingdom). The Pt content of the micelles was determined by an ion coupled plasma-mass spectrometer (4500 ICP-MS; Hewlett Packard, Palo Alto, CA).

2.5. Biodistribution

In order to analyze the fate of oxaliplatin and DACHPt/m *in vivo*, CDF_1 mice (female, n=6) were injected subcutaneously with C-26 cells (1×10^6 cells/ml). Fourteen days later, oxaliplatin or DACHPt/m prepared with PEG-*b*-P(Glu) 12–40 were intravenously injected by the tail vein at a dose of 100 μg/mouse on a platinum basis. Mice were sacrificed after defined time periods (1, 4, 8, 24, 48, and 72 h).

To assess the effect of formulation on the tissue distribution, CDF_1 mice (female, n=6) bearing s.c. C-26 tumors were intravenously administered oxaliplatin or DACHPt/m prepared with PEG-*b*-P(Glu) with different P(Glu) lengths (20, 40, and

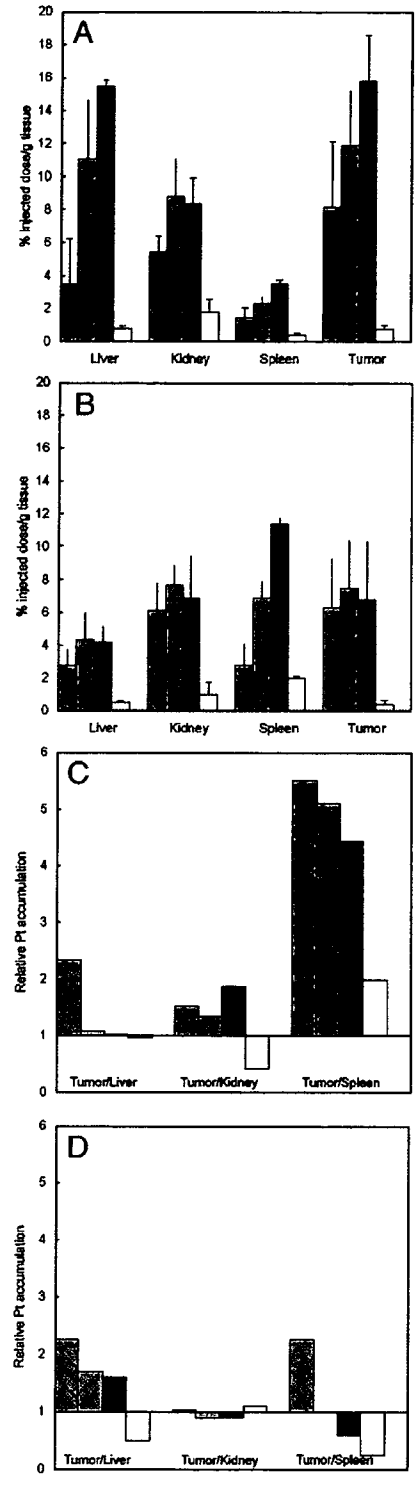

Fig. 3. Biodistribution of DACHPt-loaded micelle (DACHPt/m) prepared with PEG-*b*-P(Glu) 12–20(▨), PEG-*b*-P(Glu) 12–40(▨), PEG-*b*-P(Glu) 12–70(■) and oxaliplatin (□): A. 24 h; B.48 h; C. 24 h tumor/organ ratio; D. 48 h tumor/organ ratio. Data are expressed as averages±S.D.

70 U) at 100 μg/mouse on a platinum basis. Mice were sacrificed at 24 and 48 h post-incubation.

Tumor, liver, kidney, spleen, and muscle were collected. Blood was collected from the inferior vena cava, heparinized and centrifuged to obtain the plasma. Tissue samples were washed in ice-cold saline and weighed after removing excess fluid. All samples were dissolved in HNO_3 and evaporated to dryness. The Pt concentration was measured by ICP-MS after the samples were redissolved in 5 N HCl. The area under the curve (AUC) was calculated by the trapezoidal rule.

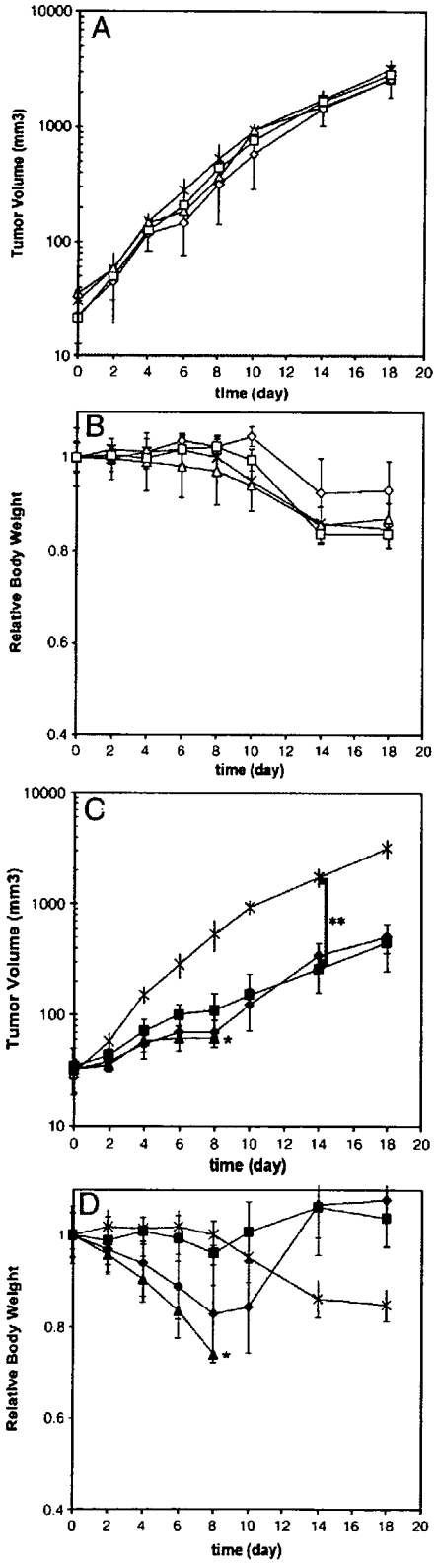

Fig. 4. Antitumor activity of DACHPt-loaded micelle (DACHPt/m) prepared with PEG-*b*-P(Glu) 12–40 against s.c. C-26 tumor model ($n=5$). Saline(×); oxaliplatin at 6 mg/kg(△); 4 mg/kg(◇); 2 mg/kg(□). DACHPt-loaded micelle (DACHPt/m) 12–40 at 6 mg/kg(▲); 4 mg/kg(◆); 2 mg/kg(■). A. Tumor volume (mm^3) for oxaliplatin treatment; B. Relative body weight of mice for oxaliplatin treatment; C. Tumor volume (mm^3) for DACHPt/m treatment; D. Relative body weight of mice for DACHPt/m treatment. Data are expressed as averages±S.D. *Toxic death. **$p<0.001$.

2.6. Antitumor activity assay

CDF_1 mice (female, $n=6$) were inoculated subcutaneously with C-26 cells (1×10^6 cells/ml). Tumors were allowed to grow for 1 week (the size of tumor at this point was approximately 30 mm^3 or 100 mm^3). Subsequently, mice were treated i.v. 4 times at 2-day intervals at doses of 2, 4, 6 and 10 mg/kg of oxaliplatin or 2, 4 and 6 mg/kg (on a platinum base) of DACHPt/m prepared with PEG-*b*-P(Glu) 12–20 or PEG-*b*-P (Glu) 12–40. The antitumor activity was evaluated in terms of tumor size (V), as estimated by the following equation:

$$V = a \times b^2/2$$

where a and b are the major and minor axes of the tumor measured by a caliper, respectively. The body weight was measured simultaneously and was taken as a parameter of systemic toxicity. The statistical analysis of animal data was carried out by the unpaired t-test.

2.7. Antitumor activity in a bioluminescent intraperitoneal metastasis model

SCID mice (female, $n=5$) were inoculated intraperitoneally with Hela-Luc cells (5×10^5 cells/ml). Tumors were allowed to grow for 3 days. Subsequently, mice were treated i.v. 3 times at 2-day intervals at doses of 4 and 6 mg/kg (on a platinum base) of oxaliplatin or DACHPt/m prepared with PEG-b-P(Glu) 12–20. *In vivo* bioluminescent imaging (BLI) was performed with an IVIS Imaging System (Xenogen) comprised of a highly sensitive, cooled CCD camera mounted in a light-tight specimen box. Images and measurements of bioluminescent signals were acquired and analyzed using Living Image software (Xenogen). Ten minutes prior to *in vivo* imaging, animals received the substrate D-luciferin (Biosynth) at 150 mg/kg in PBS by intraperitoneal injection and were anesthetized using 1–3% isoflurane (Abbott Laboratories, North Chicago, IL). Animals were placed onto a warmed stage inside the camera box and received continuous exposure to 1–2% isoflurane to sustain sedation during imaging. Imaging times ranged from 10 to 60 s, depending on the bioluminescence of the metastatic lesions. Five mice were imaged at a time. Tumor growth was monitored

by BLI every second day for 18 days. The light emitted from the bioluminescent tumors was detected *in vivo* by the IVIS Imaging System, was digitized and electronically displayed as a pseudocolor overlay onto a gray scale animal image. Regions of interest (ROI) from displayed images were drawn around the tumor sites and quantified as photons/second using the Living Image software. The statistical analysis of animal data was carried out by the unpaired *t*-test.

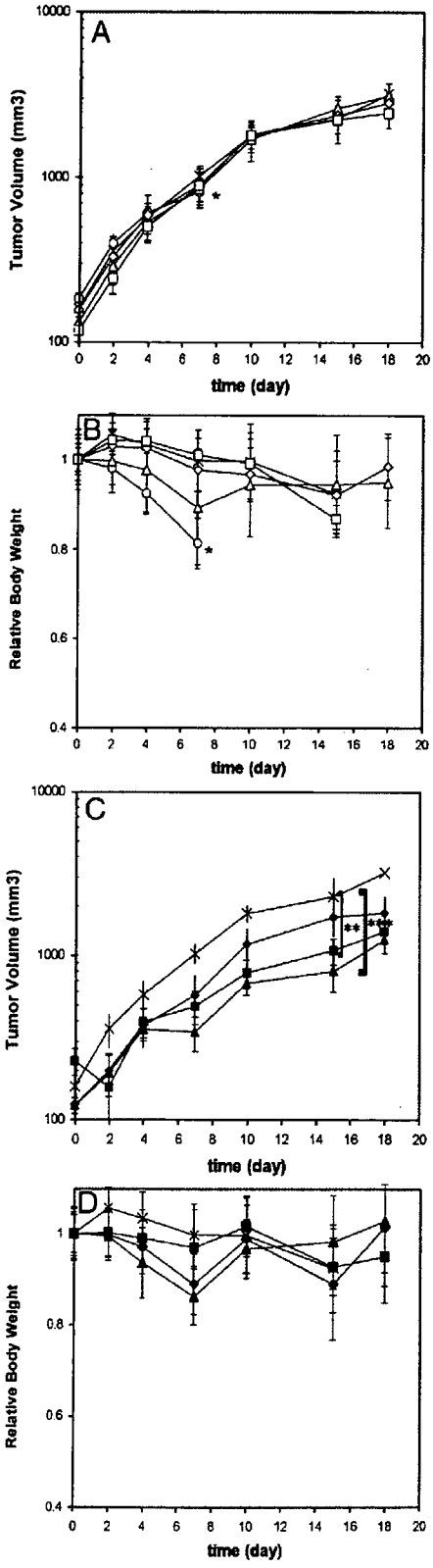

3. Results

3.1. Micelle characterization

The metal-polymer complex formation between DACHPt and the carboxylic group of the p(Glu) in the PEG-*b*-P(Glu) led to the formation of narrowly distributed micellar assemblies (Fig. 1) with average diameters of approximately 40 nm (Table 1). The increase in the length of the p(Glu) block slightly enlarged the diameter of DACHPt/m (Table 1). The drug content in the micelles was determined to be remarkably high in all the micelle formulations (Table 1). The [DACHPt]/[Glu] molar ratios in DACHPt/m were found to be similar for all the formulations.

3.2. Biodistribution

3.2.1. Biodistribution of free oxaliplatin and DACHPt/m prepared with PEG-b-P(Glu) 12–40

The biodistribution study was performed on CDF_1 mice ($n=6$) bearing s.c. C-26 tumors. Oxaliplatin or DACHPt/m prepared with PEG-*b*-P(Glu) 12–40 were i.v. injected. In previous studies, DACHPt/m prepared with PEG-*b*-P(Glu) 12–40 have shown remarkably prolonged blood circulation, whereas free oxaliplatin was promptly removed from circulation. The Pt in plasma was determined to be 15% of the injected dose at 24 h post-injection, and more than 8% even at 48 h after injection for DACHPt/m [22]. This prolonged blood circulation of DACHPt/m was reasonably associated with the high kinetic stability of the micelles in phosphate buffered saline at 37 °C [22].

The accumulations of oxaliplatin and DACHPt/m in normal tissues (kidney, liver, spleen, and muscle) and solid tumor (C-26 cells) are shown in Fig. 2. Oxaliplatin was rapidly distributed to each organ in agreement with its rapid plasma clearance. In contrast, DACHPt/m showed cumulative accumulation in each organ and solid tumor ($p<0.001$) due to its remarkably prolonged blood circulation time, and the Pt level in the liver, spleen, and tumor continuously increased up to approximately 48 h after injection (Fig. 2). Consequently, the DACHPt/m exhibited 20-, 4-, and 25-fold higher accumulation in the liver, spleen, and tumor, respectively, than oxaliplatin at 48 h after injection. To assess the selectivity to the solid tumor, the

Fig. 5. Antitumor activity of DACHPt-loaded micelle (DACHPt/m) prepared with PEG-*b*-P(Glu) 12–20 against s.c. C-26 tumor model ($n=6$). Saline(×); oxaliplatin at 10 mg/kg(○); 6 mg/kg(△); 4 mg/kg(◇); 2 mg/kg(□). DACHPt-loaded micelle (DACHPt/m) 12–20 at 6 mg/kg(▲); 4 mg/kg(◆); 2 mg/kg(■). A. Tumor volume (mm^3) for oxaliplatin treatment; B. Relative body weight of mice for oxaliplatin treatment; C. Tumor volume (mm^3) for DACHPt/m treatment; D. Relative body weight of mice for DACHPt/m treatment. Data are expressed as averages ± S.D. *Toxic death. $^{**}p<0.01$. $^{***}p<0.005$.

accumulation ratios and area under the Pt concentration-time curve (AUC) ratios of the tumor to normal tissues at 48 h after injection are summarized in Table 2. The area under the Pt concentration-time curve was calculated based on the trapezoidal rule up to 48 h. As shown in Table 2, the tumor to kidney, liver and spleen ratios were lower than 1 for oxaliplatin, suggesting no selectivity to the tumor. In contrast, the DACHPt/m exhibited accumulation and AUC ratios higher than 1.0, suggesting its selective accumulation in the tumor.

3.2.2. *Effect of P(Glu) block length on the biodistribution of micelles*

The biodistribution of the micelles prepared from PEG-*b*-P(Glu) with different p(Glu) block units in tumor-bearing mice was examined and is shown in Fig. 3. The Pt accumulation levels were studied at 24 and 48 h. All the DACHPt/m formulations showed elevated Pt levels at the tumor (Fig. 3A and B). Importantly, the amount of Pt in liver was directly correlated with the length of the p(Glu) block forming DACHPt/m. The tumor targeting efficiency of the micelles was estimated by calculating the ratio of the accumulated dose in the tumor site against the accumulated dose in the organs (Fig. 3C and D). From these results, DACHPt delivery to the tumor site by a micellar carrier seems to be extremely efficient, since all the micelles showed higher tumor/organ accumulation ratios. This efficiency was maximized for the PEG-*b*-P(Glu) 12–20-micelle formulation showing the lowest non-specific accumulation in normal tissues, thus achieving the highest relative tumor targeting. Such enhanced tumor targeting will permit expanding the therapeutic window of the micelle.

3.3. *Antitumor activity*

To evaluate the antitumor activity of DACHPt/m, CDF1 mice ($n=6$) bearing subcutaneous C-26 cells were treated i.v. four times at 2-day intervals with oxaliplatin at doses of 2, 4, 6, and 10 mg/kg or DACHPt/m (prepared with PEG-*b*-P(Glu) 12–40 and 12–20) at doses of 2, 4, and 6 mg/kg on a Pt basis. Each drug was intravenously injected on days 7, 9, 11, and 13 after inoculation, and the tumor volume after the treatment by oxaliplatin or DACHPt/m with PEG-*b*-P(Glu) 12–40 and 12–20 is shown in Figs. 4 and 5 (A and C), respectively. The relative body weight after the treatment was also monitored and shown in Figs. 4 and 5 (B and D).

The mice treated with 10 mg/kg of oxaliplatin showed toxic death after the fourth injection. Although animals treated with lower oxaliplatin doses did not show significant body weight loss, no inhibition of the tumor growth rate was observed ($p>0.05$). In contrast, the mice treated with 2 mg/kg of DACHPt/m prepared with PEG-*b*-P(Glu) 12–40 achieved significant reduction in the tumor growth rate ($p<0.001$ at day 14) without showing any body weight loss (Fig. 4C and D). Even higher tumor growth inhibition was observed for the mice treated with 4 mg/kg of PEG-*b*-P(Glu) 12–40 DACHPt/m

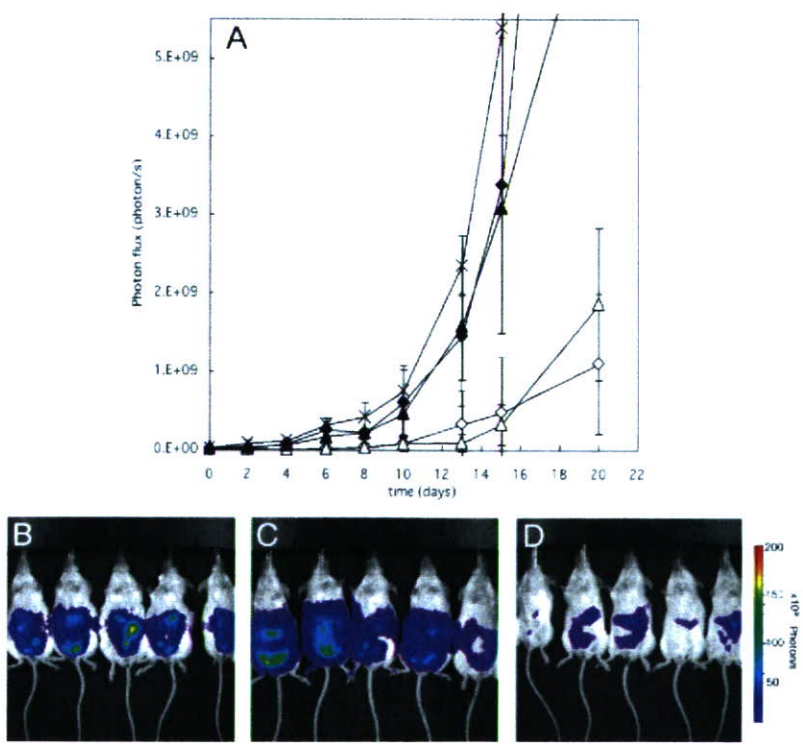

Fig. 6. Antitumor activity of DACHPt-loaded micelle (DACHPt/m) prepared with PEG-*b*-P(Glu) 12–20 against i.p. HeLa-Luc metastases ($n=5$). A. Relative photon flux from intraperitoneal metastatic sites of HeLa-luc *in vivo* treated with oxaliplatin or DACHPt-loaded micelle (DACHPt/m): Saline(×); oxaliplatin at 6 mg/kg(▲); 4 mg/kg(◆); DACHPt/m 12–20 at 6 mg/kg(△); 4 mg/kg(◇). Data are expressed as averages±S.D. *In vivo* bioluminescent images from HeLa-Luc i.p metastases at day 15: B. Saline; C. oxaliplatin 6 mg/kg; D. DACHPt/m 12–20 at 6 mg/kg.

($p<0.001$ at day 14); however, the 20% body weight loss after fourth injection suggests toxicity intensification. Increasing the DACHPt/m dose to 6 mg/kg resulted in 4 toxic deaths at day 8. The PEG-*b*-P(Glu) 12–20 micelle formulation reduced the toxicity while retaining the antitumor activity of the micelle (Fig. 5C and D). At 2 mg/kg or 4 mg/kg, this micelle formulation showed improved antitumor effect ($p<0.05$ at day 15 for 2 mg/kg; $p<0.01$ at day 15 for 4 mg/kg) compared with oxaliplatin without showing any body weight loss. At 6 mg/kg, the best tumor growth rate reduction was achieved ($p<0.005$ at day 15). The highest dose of this formulation in this experiment did not reach the lethal dose. Thus, PEG-*b*-P(Glu) 12–20 formulation for DACHPt/m seems to radically reduce drug toxicity with maintaining its potent antitumor effect, thus enlarging the therapeutic window. In addition, toxic death with DACHPt/m appeared at lower drug equivalent concentration than with oxaliplatin mainly due to the extremely high plasma AUC of DACHPt/m [22], but also because oxaliplatin is a prodrug of DACHPt. Thus, even though the drug equivalent of DACHPt/m to induce toxic death should be compared with DACHPt, it is very difficult to administer DACHPt alone due to its poor solubility.

Since DACHPt/m prepared with PEG-P(Glu) 12–70 showed higher accumulation to the liver and spleen than DACHPt/m prepared from PEG-P(Glu) 12–20 and 12–40, it will probably not increase the efficiency of the carrier. Therefore, its antitumor activity was not tested.

3.4. Antitumor activity in a bioluminescent intraperitoneal metastasis model

To evaluate the *in vivo* antitumor effect of DACHPt/m on multiple metastases generated from i.p inoculated Hela-Luc cells, SCID mice ($n=5$) were treated with free oxaliplatin or DACHPt/m beginning on day 4 post-injection. Mice with images indicating a successful i.p. inoculation on day 0 and showing *in vivo* evidence of metastasis by day 4 were placed in the drug treatment group. Free oxaliplatin or DACHPt/m were administered i.v a total of three times on day 0, 2, and 4. To quantify the bioluminescent data from metastasis, the photons emitted from the ROI in the whole animal (ventral images) were measured. The mean total photons/s were calculated from all mice. The *in vivo* bioluminescent data indicated that there was a 10-to 50-fold drop in the signal after DACHPt/m treatment (Fig. 6A). Images taken on day 15 (Fig. 6B, C, and D) indicated that DACHPt/m reduced tumor spreading in the peritoneal cavity, showing their strong growth inhibitory effect against the metastatic tumors.

4. Discussion

DACHPt/m were designed to have an extended blood circulation and a selective and high accumulation at the tumor site by the EPR effect. The average diameter of 40 nm and the hydrophilic PEG shell surrounding the micelle core are determinant features of DACHPt/m to avoid the uptake by the RES. Moreover, the sub-100 nm size of micellar nanocarriers might be optimal to achieve a remarkably high tumor extravasation efficiency and deep tumor penetration regardless of the tumor type [26]. The pharmacokinetic parameters of polymeric micelles are significantly modulated by the copolymer architecture. In this regard, the length of the micelle core-forming block not only determines the drug loading capacity of the micelle but also contributes largely to the physicochemical properties of the micelles, whereas PEG length and PEG surface density of micelles have been strongly associated with their long-circulating properties [27,28]. In this study, we prepared DACHPt/m using PEG-*b*-P(Glu) bearing different lengths of p (Glu) chain. We found that this variation considerably influences the biodistribution of micelles and thereby their antitumor activity as well as the final therapeutic window.

Drug dosage in chemotherapy is decided in part based on the competing goals of maximizing the death of malignant cells while minimizing damage to healthy cells. In the case of oxaliplatin, the major and most frequent dose-limiting toxicity observed in clinical trials was neurotoxicity [1]. Toxicological studies performed on rats with cisplatin and oxaliplatin demonstrated that the main target of neurotoxicity was the dorsal root ganglion (DRG) [29]. Although cisplatin accumulated in the DRG at a higher extent than oxaliplatin, the latter displayed more morphometric changes to the DRG after an 8-week recovery period, and this was correlated with a greater retention of oxaliplatin by the DRG in comparison with cisplatin. In contrast, neurotoxic studies revealed that CDDP-loaded micelles did not show any neurotoxicity or neuronal degeneration in rats [21]. This result might be attributed to the marked restriction of platinum accumulation into nervous tissue for the CDDP-loaded micelle, owing to the micelle size and its hydrophilic surface. Since CDDP-loaded micelles and DACHPt/m showed comparable prolonged blood circulation, preferential tumor targeting, and low accumulation in organs (Fig. 2) [20], similar reduction in the platinum accumulation at nervous tissue should be expected for DACHPt/m. Moreover, it has also been suggested that the oxalate group on oxaliplatin might immobilize calcium ions, thereby altering the amplitude of voltage-gated sodium channels of neurons [30]. The absence of an oxalate group in the DACHPt/m formulations eliminates this kind of neuronal damage.

The use of oxaliplatin is also associated with the development of severe sinusoidal injury, an aspect that had not been considered in the earlier clinical trials of oxaliplatin [31,32]. In this regard, the CDDP-loaded micelle prepared with PEG-*b*-P(Glu) 12–40 has shown transient hepatic dysfunction in rats directly related to accumulation of the micelle in liver [21]. In the present study, DACHPt/m prepared with PEG-*b*-P(Glu) 12–40 showed biphasic behavior in liver accumulation, and the Pt level in the liver remarkably increased after 8 h post-injection (Fig. 2B). Thus, the avoidance of liver uptake would be critical for the development of a clinically effective DACHPt/m formulation. We previously reported that the CDDP-loaded micelles also showed rapid accumulation of the micelle in the liver due to the morphological changes of the micelle accompanied by the release of CDDP during circulation [20]. However, such liver accumulation of the CDDP-loaded micelles was reduced for the micelle formulation from PEG-*b*-P(Glu) with a longer PEG segment [20]. Thus, the

coverage of the nanoparticles with PEG palisades is likely to be a crucial factor in the reduced liver accumulation. In this study, we evaluated the effects of the P(Glu) lengths of PEG-*b*-P(Glu) on the accumulation of the micelles in normal tissues and tumors. As a result, the micelles prepared with PEG-*b*-P(Glu) 12–20 showed considerably reduced accumulation in the liver (Fig. 3), resulting in critically reduced toxicity and, in particular, permitted a dosage increase (Fig. 5). Possibly, the use of PEG-*b*-P(Glu) with shorter P(Glu) segments may allow the formation of DACHPt/m with effective surface coverage by PEG probably due to reduced micellar core size, leading to reduction of the liver accumulation of the micelles.

DACHPt/m, prepared with PEG-b-P(Glu) 12–40 or 12–20, presented a remarkable, statistically relevant *in vivo* antitumor activity (Figs. 4 and 5), whereas free oxaliplatin failed to suppress tumor growth. The improved performance of DACHPt/m could be attributed to several aspects. The most distinguishable one is the high and preferential accumulation of DACHPt/m in the tumor due to the prolonged circulation of micelles in the bloodstream as well as the aforementioned EPR effect. In this study, DACHPt/m showed 10 times higher tumor accumulation than free oxaliplatin after 24-h post-injection, and such accumulation was maintained for an extended period (Figs. 2 and 3). On the other hand, free oxaliplatin was rapidly cleared from the bloodstream and the drug level at the tumor site was particularly low (Fig. 2). This accumulation level may be lower than the minimal amount needed to attain an efficient *in vivo* antitumor activity.

The avoidance of permanent drug inactivation by protein binding through the complexation of the platinum to the carboxylic groups in the micelle core could also be responsible for the improved biological performance of DACHPt/m over oxaliplatin. It was previously reported that, immediately after a 1 h infusion of oxaliplatin, approximately 5–30% of the drug is unbound, 10–30% is protein-bound, and 40% form complexes with hemoglobin and small molecular weight compounds in erythrocytes. Three hours later, no oxaliplatin is detectable in the plasma ultrafiltrate and only 10% is detectable in urine [33,34]. Furthermore, as many as 17 biotransformation products of oxaliplatin have been described (conjugation with methionine, cysteine, glutathione, and other low molecular weight species), but only the minor complexes $DACHPtCl_2$, $[DACHPt(H_2O)Cl]^+$ and $[DACHPt(H_2O)_2]^{2+}$ retain the ability to bind to DNA to exert the cytotoxic activity [35,36]. Among them, the dihydroxy product of oxaliplatin has been shown to have significantly greater cellular uptake and cytotoxic properties than its parent compound [37]. However, it represents a very small amount of the total plasma platinum pool after oxaliplatin administration, and therefore might not be a determinant for oxaliplatin cytotoxicity. Moreover, the formation process of $[DACHPt(H_2O)_2]^{2+}$ involves the formation of a reversible intermediate, oxalato monodentate compound, and the dissociation constant for the ring-opening step is below physiological pH (pKa=7.16). This implies that at physiological pH, the reaction favors the deprotonation of the open-ring form and the subsequent formation of the dihydroxy complex, whereas under the acidic conditions of solid tumors, ring-closure is favored and the rapid formation of oxaliplatin would be expected [38]. For DACHPt/m, the biotransformation products might be considerably different from those of oxaliplatin, and probably affect the *in vivo* performance of the drug. Since the discharge of DACHPt products from the micelle core occurs only after cleavage of the polymer-metal complex by chloride ions, and this release is enhanced at low pH, DACHPt/m probably set up conditions that favor the formation of active complexes of oxaliplatin, including the highly active $[DACHPt(H_2O)_2]^{2+}$, leading to an improved efficacy of the drug. Moreover, selective intracellular release of DACHPt complexes might occur after internalization of the micelles by endocytosis in cancer cells. As a result, DACHPt complexes may avoid extracellular inactivation and may readily induced intracellular damage.

Since systemic chemotherapy is not regarded as curative in patients with metastatic tumors and all the established therapies show low efficiency at the late stage of the disease, the antitumor activity of DACHPt/m against an i.p. metastatic tumor model was evaluated to test the potential use of micelles as a therapeutic strategy. Monitoring the development of metastatic disease is currently possible *in vivo* with the use of small animal imaging technologies including bioluminescent imaging. The results demonstrate that free oxaliplatin failed to suppress HeLa-Luc metastatic growth at any dose, whereas DACHPt/m showed a high antitumor activity while controlling tumor dissemination in the peritoneal cavity. This marked difference could be correlated to the extended blood circulation and preferential tumor accumulation of DACHPt/m, although further experiments are necessary to determine the effect of the metastatic disposition on the efficiency of the micelle. The present results revealed that DACHPt/m has a high level of antitumor activity not only on primary solid tumors but also against metastatic tumors, suggesting that DACHPt/m could be an outstanding drug delivery system for metastasis treatment.

In conclusion, we have demonstrated that decreasing the length of the core-forming block of DACHPt/m augmented their tumor specificity and drastically diminished their toxicity. Moreover, the high and preferential accumulation of the micelles at the tumor site resulted in considerable antitumor activity of DACHPt/m against primary and metastatic tumor models. Thus, DACHPt/m might be an exceptional drug delivery system for oxaliplatin active complexes.

Acknowledgments

This research was supported by a Grant-in-Aid for Scientific Research from Ministry of Education, Culture, Sports, Science and Technology of Japan as well as by the Project on the Materials Development for Innovative Nano-Drug Delivery Systems from the Ministry of Education, Culture, Sports, Science and Technology (MEXT), Japan.

References

[1] A. Ibrahim, S. Hirschfeld, M.H. Cohen, D.J. Griebel, G.A. Williams, R. Pazdur, FDA drug approval summaries: oxaliplatin, Oncologist 9 (2004) 8–12.

[2] J.M. Extra, M. Espie, F. Calvo, Phase I study of oxaliplatin in patients with advanced cancer, Cancer Chemother. Pharmacol. 25 (1990) 299–303.

[3] G. Mathé, Y. Kidani, M. Segiguchi, M. Eriguchi, G. Fredj, G. Peytavin, J.L. Misset, S. Brienza, F. de Vassals, E. Chenu, C. Bourut, Oxalato-platinum or l-OHP, a third generation platinum complex: an experimental and clinical appraisal and preliminary comparison with cis-platinum and carboplatinum, Biomed. Pharmacother. 43 (1989) 237–250.
[4] Y. Matsumura, H. Maeda, A new concept for macromolecular therapeutics in cancer chemotherapy: mechanism of tumoritropic accumulation of proteins and the antitumor agent SMANCS, Cancer Res. 46 (1986) 6387–6392.
[5] M. Yatvin, H. Miihlensiepen, W. Porschen, L. Feinendegen, J. Weinstein, Selective delivery of liposome-associated cis-dichloro-diammine platinum (II) by heat and its influence on tumor drug uptake and growth, Cancer Res. 41 (1981) 1602–1607.
[6] R. Perez-Soler, Liposomes as carriers of antitumor agents: toward a clinical reality, Cancer Treatment Rev. 16 (1989) 67–82.
[7] R. Perez-Soler, I. Han, S. Al-Baker, A.R. Khokhar, Lipophilic platinum complexes entrapped in liposomes: improved stability and preserved antitumor activity with complexes containing linear alkyl carboxylate leaving groups, Cancer Chemother. 33 (1994) 378–384.
[8] D. Avichechter, B. Schechter, R. Arnon, Functional polymers in drug delivery: carrier-supported CDDP (cis-platin) complexes carboxylates — effect on human ovarian carcinoma, React. Funct. Polym. 36 (1998) 59–69.
[9] B. Schechner, A. Newman, M. Wilnek, R. Arnon, Soluble polymers as carriers of cis-platinum, J. Control. Release 39 (1989) 75–87.
[10] X. Lin, Q. Zhang, J.R. Rice, D.R. Stewart, D.P. Nowotnik, S.B. Howell, Improved targeting of platinum chemotherapeutics. The antitumour activity of the HPMA copolymer platinum agent AP5280 in murine tumour models, Eur J Cancer. 40 (2004) 291–297.
[11] J.R. Rice, J.L. Gerberich, D. Nowotnik, S.B. Howell, Preclinical efficacy of AP5346, a novel diaminocyclohexane-platinum tumor-targeting drug delivery system, Clin. Cancer Res. 12 (2006) 2248–2254.
[12] K. Kataoka, G.S. Kwon, M. Yokoyama, Y. Sakurai, T. Okano, Block copolymer micelles as vehicles for drug delivery, J. Control. Release 24 (1993) 119–132.
[13] C. Allen, D. Mysinger, A. Eisenberg, Nano-engineering block copolymer aggregates for drug delivery, Colloids Surf., B Biointerfaces 16 (1999) 3–27.
[14] N. Nishiyama, K. Kataoka, Nano-structured devices based on block copolymer assemblies for drug delivery: designing structures for enhanced drug function, Adv. Polym. Sci. 193 (2006) 67–101.
[15] H.M. Aliabadi, A. Lavasanifar, Polymeric micelles for drug delivery, Expert Opin. Drug Deliv. 3 (2006) 139–161.
[16] N. Nishiyama, M. Yokoyama, T. Aoyagi, T. Okano, Y. Sakurai, K. Kataoka, Preparation and characterization of self-assembled polymer-metal complex micelle from cis-dichlorodiammineplatinum(II) and poly(ethylene glycol)-poly(a,b-aspartic acid) block copolymer in an aqueous medium, Langmuir 15 (1999) 377–383.
[17] N. Nishiyama, K. Kataoka, Preparation and characterization of size-controlled polymeric micelle containing cis-dichlorodiammineplatinum(II) in the core, J Control. Release 74 (2001) 83–94.
[18] N. Nishiyama, Y. Kato, Y. Sugiyama, K. Kataoka, Cisplatin-loaded polymer-metal complex micelle with time-modulated decaying property as a novel drug delivery system, Pharm. Res. 18 (2001) 1035–1041.
[19] N. Nishiyama, F. Koizumi, S. Okazaki, Y. Matsumura, K. Nishio, K. Kataoka, Differential gene expression profile between PC-14 cells treated with free cisplatin and cisplatin-incorporated polymeric micelles, Bioconjug. Chem. 14 (2003) 449–457.
[20] N. Nishiyama, S. Okazaki, H. Cabral, M. Miyamoto, Y. Kato, Y. Sugiyama, K. Nishio, Y. Matsumura, K. Kataoka, Novel cisplatin-incorporated polymeric micelles can eradicate solid tumors in mice, Cancer Res. 63 (2003) 8977–8983.
[21] H. Uchino, Y. Matsumura, T. Negishi, F. Koizumi, T. Hayashi, T. Honda, N. Nishiyama, K. Kataoka, S. Naito, T. Kakizoe, Cisplatin-incorporating polymeric micelles (NC-6004) can reduce nephrotoxicity and neurotoxicity of cisplatin in rats, Br. J. Cancer 93 (2005) 678–687.
[22] H. Cabral, N. Nishiyama, S. Okazaki, H. Koyama, K. Kataoka, Preparation and biological properties of dichloro(1,2-diaminocyclohexane)platinum (II) (DACHPt)-loaded polymeric micelles, J. Control. Release 101 (2005) 223–232.
[23] T. Tashiro, Y. Kawada, Y. Sakurai, Y. Kidani, Antitumor activity of a new platinum complex: oxalato (trans-l-diaminocyclohexane) platinum (II): new experimental data, Biomed. Pharmacother. 43 (1989) 251–260.
[24] S. Oppenheimer, Cellular basis of cancer metastasis: a review of fundamentals and new advances, Acta Histochem. 108 (2006) 327–334.
[25] Cervical cancer, NIH Consens. Statement 14 (1996) 1–38.
[26] A. Lukyanov, Z. Gao, L. Mazzola, V.P. Torchilin, Polyethylene glycol-dyacyllipid micelles demonstrate increased accumulation in subcutaneous tumors in mice, Pharm. Res. 19 (2002) 1424–1429.
[27] G.S. Kwon, S. Suwa, M. Yokoyama, T. Okano, Y. Sakurai, K. Kataoka, Enhanced tumor accumulation and prolonged circulation times of micelles-forming poly(ethyleneoxide-aspartate) block copolymers-adriamycin conjugates, J. Control. Release 29 (1994) 17–23.
[28] M. Yokoyama, T. Okano, Y. Sakurai, S. Fukushima, K. Okamoto, K. Kataoka, Selective delivery of adriamycin to a solid tumor using a polymeric micelle carrier system, J. Drug Target. 7 (1999) 171–186.
[29] G. Cavaletti, G. Tredici, M.G. Petruccioli, E. Donde, P. Tredici, P. Marmiroli, C. Minoia, A. Ronchi, M. Bayssas, G. Griffon Etienne, Effects of different schedules of oxaliplatin treatment on the peripheral nervous system of the rat, Eur. J. Cancer 37 (2001) 2457–2463.
[30] F. Grolleau, L. Gamelin, M. Boisdron-Celle, B. Lapied, M. Pelhate, E. Gamelin, A possible explanation for a neurotoxic effect of the anticancer agent oxaliplatin on neuronal voltage-gated sodium channels, J. Neurophysiol. 85 (2001) 2293–2297.
[31] L. Rubbia-Brandt, V. Audard, P. Sartoretti, A.D. Roth, C. Brezault, M. Le Charpentier, B. Dousset, P. Morel, O. Soubrane, S. Chaussade, G. Mentha, B. Terris, Severe hepatic sinusoidal obstruction associated with oxaliplatin based chemotherapy in patients with metastatic colorectal cancer, Ann. Oncol. 15 (2004) 460–466.
[32] G. Tisman, D. MacDonald, N. Shindell, E. Reece, P. Patel, N. Honda, E.K. Nishimora, J. Garris, W. Shannahan, N. Chisti, J. McCarthy, S.N. Moaddeli, D. Sargent, A. Plant, Oxaliplatin toxicity masquerading as recurrent colon cancer, J. Clin. Oncol. 22 (2004) 3202–3204.
[33] J. Liu, E. Kraut, J. Bender, R. Brooks, S. Balcerzak, M. Grever, H. Stanley, S. D'Ambrosio, R. Gibson-D'Ambrosio, K.K. Chan, Pharmacokinetics of oxaliplatin (NSC266046) alone and in combination with paclitaxel in cancer patients, Cancer Chemother. Pharmacol. 49 (2002) 367–374.
[34] C. Massari, S. Brienza, M. Rotarski, J. Gastiaburu, J.-L. Misset, D. Cupissol, E. Alafaci, H. Dutertre-Catella, G. Bastian, Pharmacokinetics of oxaliplatin in patients with normal versus impaired renal function, Cancer Chemother. Pharmacol. 45 (2000) 157–164.
[35] F.R. Luo, S.D. Wyrick, S.G. Chaney, Biotransformations of oxaliplatin in rat blood *in vitro*, J. Biochem. Molec. Toxicol. 13 (1999) 159–169.
[36] F.R. Luo, T.-Y. Yen, S.D. Wyrick, S.G. Chaney, High-performance liquid chromatographic separation of the biotransformation products of oxaliplatin, J. Chromatogr., B 724 (1999) 345–356.
[37] F.R. Luo, S.D. Wyrick, S.G. Chaney, Cytotoxicity, cellular uptake and cellular biotransformations of oxaliplatin in human colon carcinoma cells, Oncol. Res. 10 (1998) 595–603.
[38] E. Jerremalm, P. Videhult, G. Alvelius, W.J. Griffiths, T. Bergman, S. Eksborg, H. Ehrsson, Alkaline hydrolysis of oxaliplatin — isolation and identification of the oxalato monodentate intermediate, J. Pharm. Sci. 91 (2002) 2116–2121.

Cyclic RGD Peptide-Conjugated Polyplex Micelles as a Targetable Gene Delivery System Directed to Cells Possessing $\alpha_v\beta_3$ and $\alpha_v\beta_5$ Integrins

Makoto Oba,[†] Shigeto Fukushima,[‡,§] Naoki Kanayama,[§,¶] Kazuhiro Aoyagi,[§] Nobuhiro Nishiyama,[#] Hiroyuki Koyama,[†] and Kazunori Kataoka*[,§,¶,#,⊥]

Department of Clinical Vascular Regeneration, Graduate School of Medicine, The University of Tokyo, 7-3-1 Hongo, Bunkyo, Tokyo 113-8655, Japan, R&D Division, Pharmaceuticals Group, Nippon Kayaku Co., Ltd., Department of Materials Engineering, Graduate School of Engineering, The University of Tokyo, 7-3-1 Hongo, Bunkyo, Tokyo 113-8656, Japan, CREST, Japan Science and Technology Agency, Japan, Center for Disease Biology and Integrative Medicine, Graduate School of Medicine, The University of Tokyo, 7-3-1 Hongo, Bunkyo, Tokyo 113-0033, Japan, and Center for NanoBio Integration, The University of Tokyo, 7-3-1 Hongo, Bunkyo, Tokyo 113-8656, Japan. Received January 15, 2007; Revised Manuscript Received May 11, 2007

A cyclic RGD peptide-conjugated block copolymer, cyclo[RGDfK(CX-)]−poly(ethylene glycol)−polylysine (c(RGDfK)−PEG−PLys), was synthesized from acetal-PEG−PLys under mild acidic conditions and spontaneously associated with plasmid DNA (pDNA) to form a polyplex micelle in aqueous solution. The cyclic RGD peptide recognizes $\alpha_v\beta_3$ and $\alpha_v\beta_5$ integrin receptors, which play a pivotal role in angiogenesis, vascular intima thickening, and the proliferation of malignant tumors. The c(RGDfK)−PEG−PLys/pDNA polyplex micelle showed a remarkably increased transfection efficiency (TE) compared to the PEG−PLys/pDNA polyplex micelle for the cultured HeLa cells possessing $\alpha_v\beta_3$ and $\alpha_v\beta_5$ integrins. On the other hand, in the transfection against the 293T cells possessing no $\alpha_v\beta_3$ and a few $\alpha_v\beta_5$ integrins, the TE of the c(RGDfK)−PEG−PLys/pDNA micelle showed no increase compared to the TE of the PEG−PLys/pDNA micelle. Flow cytometric analysis revealed a higher uptake of the c(RGDfK)−PEG−PLys/pDNA micelle than the PEG−PLys/pDNA micelle against HeLa cells, consistent with the transfection results. Furthermore, a confocal laser scanning microscopic observation revealed that the pDNA in the c(RGDfK)−PEG−PLys micelle preferentially accumulated in the perinuclear region of the HeLa cells within 3 h of incubation. No such fast and directed accumulation of pDNA to the perinuclear region was observed for the micelles without c(RGDfK) ligands. These results indicate that the increase in the TE induced by the introduction of the c(RGDfK) peptide ligand was due to an increase in cellular uptake as well as facilitated intracellular trafficking of micelles toward the perinuclear region via $\alpha_v\beta_3$ and $\alpha_v\beta_5$ integrin receptor-mediated endocytosis, suggesting that the cyclic RGD peptide-conjugated polyplex micelle has promising feasibility as a site-specifically targetable gene delivery system.

INTRODUCTION

With the increase in available information on various disease genes that has resulted from progress in the Human Genome Project, gene therapy is increasingly recognized as a promising therapy for many intractable diseases. Obviously, a major key to successful gene therapy is the development of gene vectors that are particularly effective for *in vivo* use. Nevertheless, there are many restrictions in the clinical application of viral vectors, which have played a pivotal role in gene therapy up to now, because of their safety issues, including antigenicity, as well as to the difficulty of formulating them with good quality control. These limitations of viral vectors have led to the recent trend in developing nonviral vectors with safety and high productivity as alternative systems to viral vectors.

One of the important challenges in the development of nonviral vectors is the system available for systemic injection, which must be stable enough to achieve longevity in the blood circulation but also be able to achieve high transfection efficiency (TE) in the target region with minimal toxicity. Lipoplex (*1*) and polyplex (*2*) systems based on cationic lipids and polymers, respectively, have been extensively studied as nonviral gene vectors for systemic administration. Nevertheless, there remain unresolved issues with these systems, because it is generally required that they contain excessive cationic lipids or polymers to increase solubility in an aqueous solution. Eventually, shifting their surface charge to a positive value induces nonspecific interaction with anionic components in the body such as plasma proteins and blood cells. This apparently hampers their applicability to systemic gene delivery. Polyplex micelles (*3*), characterized by the unique core−shell architecture of the hydrophilic shell layer surrounding their polyplex core, have the potential to acquire a so-called "stealth" property to minimize nonspecific interaction with biocomponents. Indeed, a polyplex micelle with poly(ethylene glycol) (PEG) as a hydrophilic shell layer achieved high stability in a medium containing serum compared to conventional lipoplexes and polyplexes and showed increased retention time in the bloodstream (*4*, *5*), suggesting that a polyplex micelle may be a promising candidate for a vector that can be used in systemic gene delivery. Nevertheless, in order to increase selective uptake into the target cells, appropriate ligands are preferably introduced into the surface of the polyplex micelles. In this way, surface-installed ligands are expected to enhance the uptake rate of the

* To whom correspondence should be addressed. Tel: +81-3-5841-7138, fax: +81-3-5841-7139, e-mail: kataoka@bmw.t.u-tokyo.ac.jp.
† Department of Clinical Vascular Regeneration, The University of Tokyo.
‡ Nippon Kayaku Co., Ltd.
§ Department of Materials Engineering, The University of Tokyo.
¶ CREST.
# Graduate School of Medicine, The University of Tokyo.
⊥ Center for NanoBio Integration, The University of Tokyo.

10.1021/bc0700133 CCC: $37.00
Published on Web 06/27/2007

polyplex micelles into the target cells by receptor-mediated endocytosis, which may lead to higher gene TE compared to the ligand-free polyplex micelles taken up by the cells through adsorptive or fluid-phase endocytosis (*6*–*8*).

In this study, acetal-poly(ethylene glycol)–polylysine (acetal-PEG–PLys) was synthesized as a precursor for constructing ligand-installed polyplex micelles. PLys, which is one of the first polymers used and well studied as a nonviral vector, was chosen as a cationic segment of the block copolymer. PLys-based polyplexes are known to show a relatively low TE against cultured cell lines compared to those having the endosomal escape function, such as polyethylenimine (PEI)-based polyplexes, but they have an advantage in stability even in a diluted condition, and they have shown an appreciable level of gene transfection in animal models (*5*, *9*). A cyclic RGD peptide (c(RGDfK)), which selectively recognizes $\alpha_v\beta_3$ and $\alpha_v\beta_5$ integrin receptors (*10*), was chosen as a ligand and introduced into the PEG terminus of aldehyde-PEG–PLys, derived from acetal-PEG–PLys, through a thiazolidine ring formation, and the c(RGDfK)–PEG–PLys block copolymer was obtained. It is generally known that the $\alpha_v\beta_3$ and $\alpha_v\beta_5$ integrins are expressed on various cell types such as endothelial cells, osteoclasts, macrophages, platelets, and melanomas, and that they play a significant role in angiogenesis, vascular intima thickening, and the proliferation of malignant tumors (*11*). Therefore, gene delivery targeting the $\alpha_v\beta_3$ and $\alpha_v\beta_5$ integrins is expected to be useful in the treatment of cancer and vascular diseases. Indeed, the c(RGDfK)–PEG–PLys/pDNA polyplex micelle thus prepared showed a remarkably increased TE compared to ligand-free polyplex micelles against the HeLa cells expressing $\alpha_v\beta_3$ and $\alpha_v\beta_5$ integrins.

EXPERIMENTAL PROCEDURES

Materials. 3,3-Diethoxypropanol was purchased from Aldrich Chemical Co. Ltd. (Milwaukee, WI). Ammonia solution (25%), tetrahydrofuran (THF), *N,N*-dimethylformamide (DMF), *n*-hexane, methanesulfonyl chloride (MsCl), and triethylamine (TEA) were purchased from Wako Pure Chem. Co. Ltd. (Japan). Ethylene oxide (EO) was purchased from Sumitomo Seika Chemicals Co. Ltd. (Japan). THF was distilled according to the conventional procedure as previously reported (*12*). DMF was dehydrated using activated molecular sieves (4A) and distilled under reduced pressure. 3,3-Diethoxypropanol and *n*-hexane were distilled over sodium wire. MsCl, TEA, and EO were dried over calcium hydride followed by distillation. CXYGGRGDS (RGDS) and cyclo[RGDfK(CX-)] (c(RGDfK)) peptides (X = 6-aminocaproic acid; ϵ-Acp) were purchased from Peptide Institute, Inc. (Japan). The PEG–PLys block copolymer (PEG; 12 000 g/mol, polymerization degree of PLys segment; 73) was synthesized as previously reported (*13*). A micro BCA protein assay reagent kit was purchased from Pierce (Rockford, IL). The Luciferase assay kit was a product of Promega (Madison, WI). Plasmid pCAcc+Luc coding for firefly luciferase under the control of the CAG promoter was provided by the RIKEN Gene Bank (Japan), amplified in competent DH5α *Escherichia coli*, and then purified using a HiSpeed Plasmid MaxiKit purchased from QIAGEN Sciences Co., Inc. (Germany). FITC-labeled monoclonal antibodies against $\alpha_v\beta_3$ integrin, $\alpha_v\beta_5$ integrin, and mouse IgG were purchased from Cosmo Bio Co., Ltd. (Japan). QuantiLum recombinant luciferase was purchased from Promega (Madison, WI).

Measurements. Gel permeation chromatography (GPC) measurements were carried out using a TOSOH HLC-8220 equipped with TSKgel columns (G4000PWXL and G3000PWXL). The internal refractive index (RI) was used for detection of the polymer. DMF with 10 mM LiCl was used as an eluent at a flow rate of 0.8 mL min^{-1} at 40 °C. IR was measured with an IR Report-100 spectrometer (JASCO, Tokyo, Japan). ^1H NMR spectra were obtained with a JEOL EX300 spectrometer (JEOL, Tokyo, Japan). Chemical shifts are reported in ppm relative to the residual protonated solvent resonance.

Synthesis of RGDS–PEG–PLys 5a and c(RGDfK)–PEG–PLys 5b (Scheme 1). *Acetal-PEG-NH_2 2.* A THF solution of 3,3-diethoxypropanol (0.16 mL, 1 mmol) and potassium naphthalene (2.7 mL, 0.90 mmol) were mixed in THF (75 mL) to form potassium 3,3-diethoxypropanolate (PDP) as previously reported (*14*). After the mixture was stirred for 10 min, liquid EO (13.5 mL, 270 mmol) chilled below 0 °C was added to the solution with additional stirring at room temperature (r.t.) for 2 days. The reactant polymer was isolated by precipitation into diethyl ether and lyophilized from benzene to obtain acetal-PEG-OH (12.65 g, quant). Acetal-PEG-OH (6.01 g, 0.50 mmol) was then dissolved in THF (40 mL), followed by the addition of TEA (0.32 mL, 2.25 mmol). Subsequently, the solution was slowly added dropwise into MsCl (0.12 mL, 1.5 mmol) in THF (20 mL) and stirred at 0 °C for 2 h. The solution was poured into diethyl ether to precipitate acetal-PEG-OMs **1**. The recovered acetal-PEG-OMs **1** was dissolved in 25% ammonia solution (500 mL) and stirred at r.t. for 4 days. The volume of the solution was concentrated to 50 mL by evaporation and dialyzed sequentially against 0.125% ammonia solution and distilled water, followed by lyophilization to obtain acetal-PEG-NH_2 **2** (5.40 g, 90%).

Acetal-PEG–PLys(TFA) 3. N^{ϵ}-Trifluoroacetyl-L-lysine *N*-carboxyanhydride (Lys(TFA)-NCA) (3.59 g, 13.39 mmol, 80 equiv to **2**) prepared according to the protocol described in the literature (*15*) in DMF (40 mL) was added to acetal-PEG-NH_2 **2** (2.01 g, 167.5 μmol) in DMF (20 mL) and stirred at 40 °C for 2 days. The polymerization was monitored by IR. The reactant polymer was precipitated into AcOEt/hexane (4:6) and lyophilized in dioxane to obtain acetal-PEG–PLys(TFA) **3** (4.08 g, 73%).

Acetal-PEG–PLys 4. NaOH solution (1 N, 4 mL) was added to acetal-PEG–PLys(TFA) **3** (500 mg, 17.77 μmol) in MeOH (40 mL) and stirred at 40 °C for 24 h. The reacted polymer was purified by dialysis sequentially against 10 mM PBS solution (pH 7.0) and distilled water and lyophilized to obtain acetal-PEG–PLys **4** (498 mg, quant).

*RGDS–PEG–PLys **6a** and c(RGDfK)–PEG–PLys **6b**.* Conjugation of the peptide into the PEG terminus of PEG–PLys was performed through thiazolidine ring formation using RGDS or c(RGDfK) peptide. RGDS–PEG–PLys **6a** was synthesized according to the typical procedure, as follows: Acetal-PEG–PLys **4** (39.1 mg, 1.64 μmol) was added to RGDS (15.2 mg, 16.4 μmol) in 0.2 M AcOH buffer (pH 4.0, 8 mL) and stirred at room temperature for 5 days. The reacted polymer was purified by dialysis sequentially against 10 mM PBS solution (pH 7.0) and distilled water and lyophilized to obtain RGDS–PEG–PLys **6a** (35.4 mg, 86%). Conjugation of the c(RGDfK) to acetal-PEG–PLys **4** was carried out in a similar way, e.g., c(RGDfK) (7.4 mg, 9.03 μmol) and acetal-PEG–PLys **4** (30.0 mg, 1.26 μmol) were used to obtain c(RGDfK)–PEG–PLys **6b** (26.6 mg, 87%).

Preparation of Polyplex Micelles. Each block copolymer and pDNA was dissolved separately in 10 mM Tris-HCl buffer (pH 7.4). The polymer solution in varying concentrations was added to a twice-excess volume of pDNA solution to form polyplex micelles with different compositions. The final pDNA concentration was adjusted to 33.3 or 50 μg/mL. The resulting solution was kept at r.t. overnight. The N/P ratio was defined as the residual molar ratio of the amino groups of PLys units to the phosphate groups of pDNA.

Ethidium Bromide Exclusion Assay. Polyplex micelle solutions (50 μg pDNA/mL) prepared at various N/P ratios were

Scheme 1. Syntheses of RGDS−PEG−PLys 6a and c(RGDfK)−PEG−PLys 6b

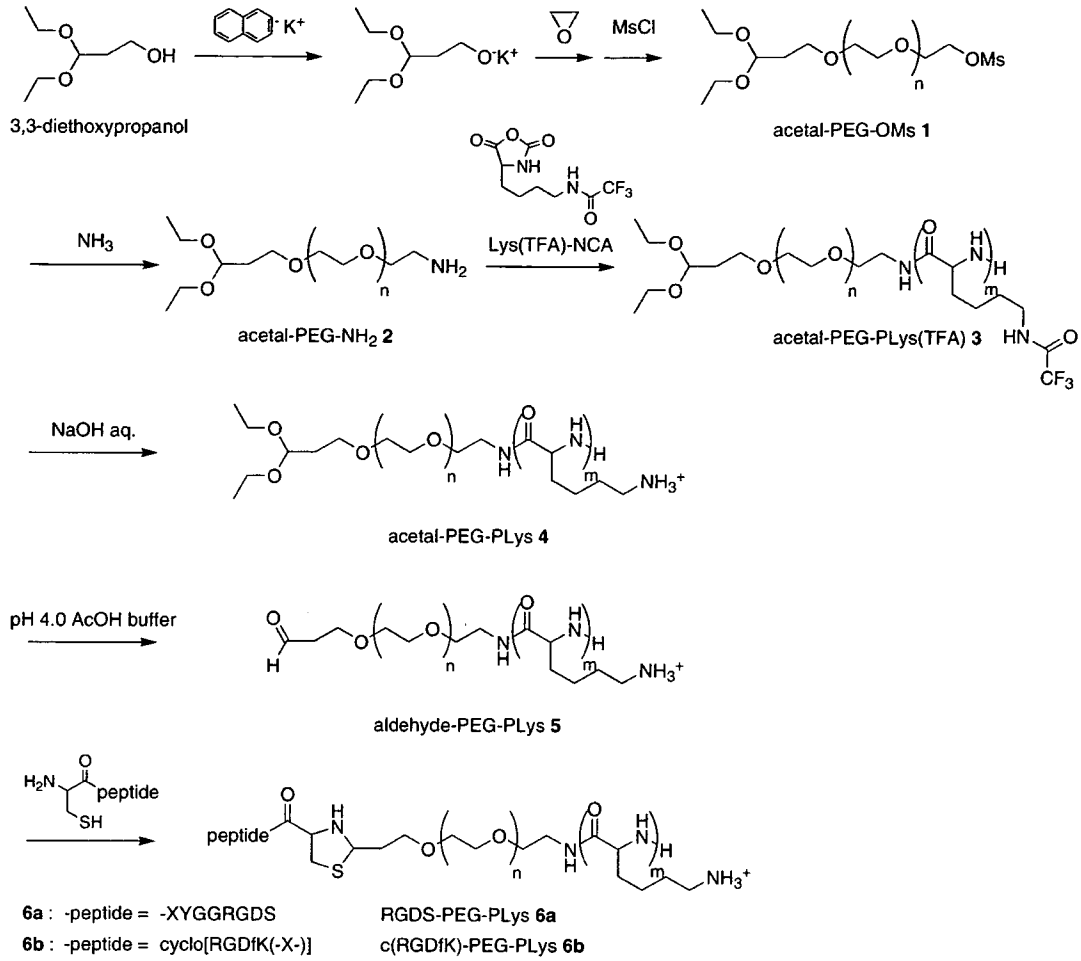

adjusted to contain 10 μg pDNA/mL with 2.5 μg ethidium bromide (EtBr)/mL and 150 mM NaCl by adding 10 mM Tris-HCl solution (pH 7.4) containing EtBr and NaCl. The solutions were kept at r.t. overnight. The fluorescence intensity of the sample solutions at 590 nm (excitation wavelength: 365 nm) was measured at 25 °C using a spectrofluorometer (ND-3300, NanoDrop, Wilmington, DE). The fluorescence intensity of naked pDNA was set at 100% and measured against a background of EtBr without pDNA.

Dynamic Light Scattering Measurement. The size of the polyplex micelles was evaluated by dynamic light scattering (DLS) using Nano ZS (ZEN3600, Malvern Instruments, Ltd., UK). A He−Ne ion laser (633 nm) was used as the incident beam. Polyplex micelle solutions (50 μg pDNA/mL) with an N/P = 2 were adjusted to a concentration of 10 μg pDNA/mL. The data obtained at a detection angle of 173 ° at 25 °C were analyzed by a cumulant method to obtain the hydrodynamic diameters and polydispersity indices (μ/Γ^2) of the micelles. The results reported are expressed as the mean values (±SEM) of three experiments.

ζ-Potential Measurement. The ζ-potential of polyplex micelles was evaluated by the laser-doppler electrophoresis method using Nano ZS with a He−Ne ion laser (633 nm). Sample solutions similar to those used for the DLS measurements were prepared. The ζ-potential measurements were carried out at 25 °C. A scattering angle of 17° was used in these measurements. The results are expressed as the mean values (±SEM) of three experiments.

Detection of $\alpha_v\beta_3$ and $\alpha_v\beta_5$ Integrin Receptors. 293T cells and HeLa cells were detached by pipetting and by harvesting with trypsin, respectively. Both types of cells were washed twice with PBS. The 1 × 10^6 cells and FITC-labeled antibody against $\alpha_v\beta_3$ or $\alpha_v\beta_5$ integrin (2 μg) were resuspended in 100 μL of Dulbecco's Modified Eagle Medium (DMEM) (containing 10% serum) and incubated on ice for 1 h in the dark. The cells were washed three times with cold medium and, after being resuspended in PBS, were analyzed using a flow cytometer (EPICS XL, Beckman Coulter, Inc.). The cytometric data were analyzed using EXPO32 software (Beckman Coulter, Inc., Fullerton, CA).

Transfection. HeLa and 293T cells were respectively seeded on 24-well culture plates (10 000 cells/well) and incubated overnight in 500 μL of DMEM containing 10% serum. After the medium was replaced with fresh medium, 20 μL of polyplex solution (50 μg pDNA/mL, N/P = 2) was applied to each well. The amount of pDNA was adjusted to 1 μg per well. After incubation for various lengths of time, the medium was replaced with 500 μL of fresh medium, followed by reincubation. The reincubation time was adjusted so the total incubation time would be 48 h. The luciferase gene expression was then evaluated based on the intensity of the photoluminescence using the Luciferase assay kit and a Luminometer (Lumat LB9507, BERTHOLD, Germany). The amount of protein in each well was concomitantly determined using a Micro BCA protein assay reagent kit. The relative light units were converted into the absolute amount of luciferase (ng) using a standard curve calibrated with recombinant luciferase (QuantiLum, Promega). One nanogram of luciferase corresponded to 9.1 × 10^7 RLU in our experiments; this was defined as the conversion factor.

Analysis of Cellular Uptake of Polyplex Micelles. pDNA was labeled with fluorescein as previously reported (*4*). Briefly,

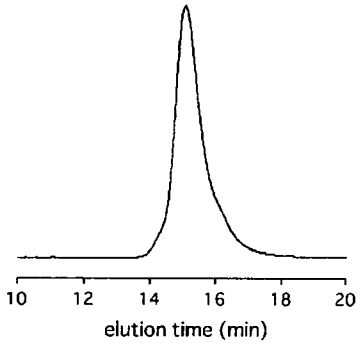

Figure 1. Gel permeation chromatogram of acetal-PEG–PLys(TFA) **3** (instrument TOSOH HLC-8220, detector RI, columns TSKgel G4000PWXL and G3000PWXL, eluent DMF with 10 mM LiCl, flow rate 0.8 mL min^{-1}, temperature 40 °C).

pDNA was labeled using a Label IT Nucleic Acid Labeling Kit (Mirus, Madison, WI). HeLa cells were seeded on six-well culture plates (100 000 cells/well) and incubated overnight in 1 mL of DMEM containing 10% serum. After the medium was replaced with fresh medium, 90 μL of polyplex solution (33.3 μg fluorescein-labeled pDNA/mL, N/P = 2) was applied to each well. The amount of fluorescein-labeled pDNA was adjusted to 3 μg per well. After various periods of incubation, the medium was removed and the cells were washed twice with PBS. After detachment by trypsin, the cells were resuspended in PBS and analyzed using the flow cytometer.

Confocal Laser Scanning Microscope (CLSM) Observation. pDNA was labeled with Cy5 in the same manner as fluorescein using the Label IT Nucleic Acid Labeling Kit. HeLa cells (30 000 cells) were seeded on a 35-mm glass base dish (Iwaki, Japan) and incubated overnight in 1 mL of DMEM containing 10% serum. After the medium was replaced with fresh medium, 90 μL of polyplex solution containing 3 μg Cy5-labeled pDNA (N/P = 2) was applied to a glass dish. After 3 h incubation, the medium was removed and the cells were washed twice with PBS. The intracellular distributions of the polyplex micelles were observed by CLSM following acidic late endosome and lysosome staining with LysoTracker Green (Molecular Probes, Eugene, OR) and nuclear staining with Hoechst 33342 (Dojindo Laboratories, Japan). The CLSM observation was performed using LSM 510 (Carl Zeiss, Germany) with a 63× objective (C-Apochromat, Carl Zeiss, Germany) at excitation wavelengths of 488 nm (Ar laser), 633 nm (He–Ne laser), and 710 nm (Mai Tai laser) for fluorescein, Cy5, and Hoechst 33342, respectively.

RESULTS

Synthesis of Peptide-Conjugated PEG–PLys (Scheme 1). The synthesis of acetal-PEG-OMs **1** has been previously reported (*14*). Briefly, PDP from 3,3-diethoxypropanol and potassium naphthalene initiated the anionic polymerization of EO to form acetal-PEG-OH (M_n 11 825, M_w 12 089, M_w/M_n 1.02), followed by the mesylation of alcohol using MsCl to obtain acetal-PEG-OMs **1**. Acetal-PEG-NH_2 **2** was then synthesized by amination of acetal-PEG-OMs **1** using ammonia solution and was confirmed to be unimodal with a narrow molecular weight distribution (M_w/M_n 1.03). Polymerization of Lys(TFA)-NCA using acetal-PEG-NH_2 **2** as an initiator led to the formation of acetal-PEG–PLys(TFA) **3**. A GPC of the obtained acetal-PEG–PLys(TFA) **3** showed a single peak with a narrow molecular weight distribution (M_w/M_n 1.12) (Figure 1). From the peak intensity ratio of the methylene protons of PEG (OCH_2CH_2, δ = 3.6 ppm) and the methylene protons of Lys(TFA) ($CH_2CH_2CH_2CH_2NH$, δ = 1.4, 1.5, 1.9, and 3.2 ppm) measured by ^{1}H NMR, the polymerization degree (DP) of Lys-

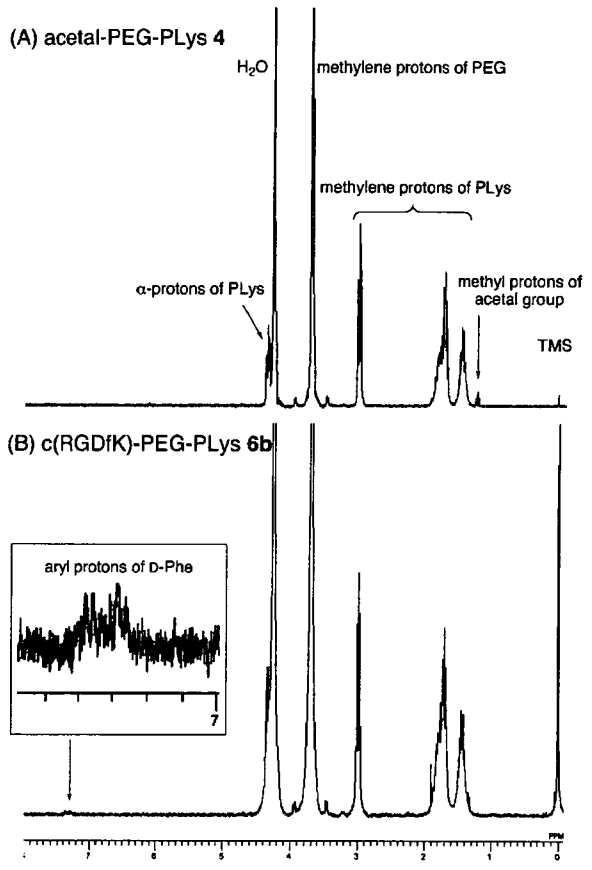

Figure 2. ^{1}H NMR spectra of acetal-PEG–PLys **4** (A) and c(RGDfK)–PEG–PLys **6b** (B) in D_2O at 80 °C.

(TFA) was calculated to be 70 (data not shown). Acetal-PEG–PLys **4** was then quantitatively obtained by the deprotection of acetal-PEG–PLys(TFA) **3** under basic conditions. From the ^{1}H NMR spectrum, the acetal group (CH_3CH_2O, δ = 1.2 ppm) was confirmed to be almost intact without converting to an aldehyde group (Figure 2). The DP of Lys was calculated to be 72 from the peak intensity ratio of the methylene protons of PEG (OCH_2CH_2, δ = 3.6 ppm) and the methylene protons of PLys ($CH_2CH_2CH_2CH_2NH_3$, δ = 1.4, 1.7, and 3.0 ppm) (Figure 2). The DP of acetal-PEG–PLys(TFA) **3** and acetal-PEG–PLys **4** were almost identical, indicating that main chain cleavage under the deprotection reaction was negligible.

Conjugation of peptide ligands into the PEG terminus of acetal-PEG–PLys **4** was achieved through the formation of a thiazolidine ring. The acetal group was deprotected under acidic conditions to an aldehyde group, giving aldehyde-PEG–PLys **5**. The aldehyde group is known to react with cysteine to form a stable thiazolidine ring (*16*). In this study, CXYGGRGDS (RGDS) and cyclo[RGDfK(CX-)] (c(RGDfK)), having an N-terminal cysteine residue (C: L-Cys), were reacted with acetal-PEG–PLys **4** under mild acidic conditions (pH 4.0) to prepare the peptide-conjugated PEG–PLys through thiazolidine formation. Note that Schiff base formation due to the reaction of the aldehyde and primary amino groups of the PLys segment was prohibited under the acidic conditions because of the complete protonation of the primary amino groups. The methyl protons of the acetal group (δ = 1.2 ppm) completely disappeared with the appearance of protons assigned to the aromatic rings of L-tyrosine (Y: L-Tyr:) (δ = 6.9 and 7.1 ppm) in the RGDS and D-phenylalanine (f: D-Phe) (δ = 7.3 and 7.4 ppm) in the c(RGDfK) (Figure 2). Based on the peak intensity ratios of the aromatic ring protons of peptide ligands and the methylene

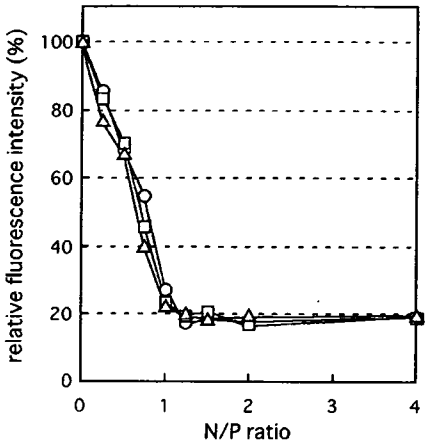

Figure 3. Ethidium bromide exclusion assays of PEG−PLys (open circle), RGDS−PEG−PLys (open square), and c(RGDfK)−PEG−PLys (open triangle). Fluorescence measurements were carried out as described in the Experimental Procedures.

Table 1. Size and ζ-Potentials of Polyplex Micelles

sample	cumulant diameter (nm)/ polydispersity index (μ/Γ^2)	ζ-potential (mV)
PEG−PLys	124 ± 0.27/0.158 ± 0.014	−0.19 ± 0.195
RGDS−PEG−PLys	124 ± 0.88/0.177 ± 0.012	1.12 ± 0.349
c(RGDfK)−PEG−PLys	125 ± 1.00/0.166 ± 0.006	0.68 ± 0.238

protons of PEG (OCH_2CH_2, δ = 3.6 ppm), the introduction rates of peptide ligands were determined to be 100% in the RGDS−PEG−PLys **6a** and 66% in the c(RGDfK)−PEG−PLys **6b**.

Formation of Polyplex Micelles. Ethidium bromide (EtBr) is known to form an intercalating complex with double helical polynucleotides and subsequently show a striking enhancement of its fluorescence intensity (*17*). This enhancement is quenched by the formation of a complex between DNA and cationic components, because cationic components prevent EtBr from intercalating into the double-strand DNA. Thus, EtBr exclusion assay is frequently utilized to estimate the degree of pDNA condensation in the complex with a catiomer (*18*, *19*). As shown in Figure 3, as the N/P ratio increased, the fluorescence intensity in all the polyplex micelles decreased correspondingly and leveled off at around N/P = 1.25. This result indicates that the degree of pDNA condensation was not influenced by the introduction of peptide ligands. Table 1 summarizes the cumulant diameters and ζ-potentials of the polyplex micelles at N/P = 2. The cumulant diameters of all the micelles were approximately 125 nm with a moderate polydispersity index between 0.15 and 0.18. There was no change in the particle size because of the introduction of peptide ligands. Also, the ζ-potentials of all the polyplex micelles were approximately 0 mV. As previously reported (*5*, *18*), the PEG palisade surrounding the complex shields the charge of the micelles to maintain a very small absolute value in the ζ-potential even in the region of N/P > 1. All of the results of the EtBr assay, DLS analysis, and ζ-potential measurement suggest that the characteristics of the three types of polyplex micelles (PEG−PLys, RGDS−PEG−PLys, and c(RGDfK)−PEG−PLys) were quite similar regardless of the introduction of the peptide ligands.

Detection of $\alpha_v\beta_3$ and $\alpha_v\beta_5$ Integrin Receptors. To evaluate the expression of integrin receptors on the cell surface, flow cytometric analysis of 293T and HeLa cells was carried out using FITC-labeled antibodies (Figure 4). Flow cytometric analysis revealed that the 293T cells expressed almost no $\alpha_v\beta_3$ integrin and a slight amount of $\alpha_v\beta_5$ integrin, while the HeLa cells expressed a considerably higher amount of $\alpha_v\beta_3$ and $\alpha_v\beta_5$ integrins than the 293T cells. These results implied that HeLa cells might show a higher uptake of the cyclic RGD peptide-conjugated polyplex micelles than 293T cells through integrin-mediated endocytosis.

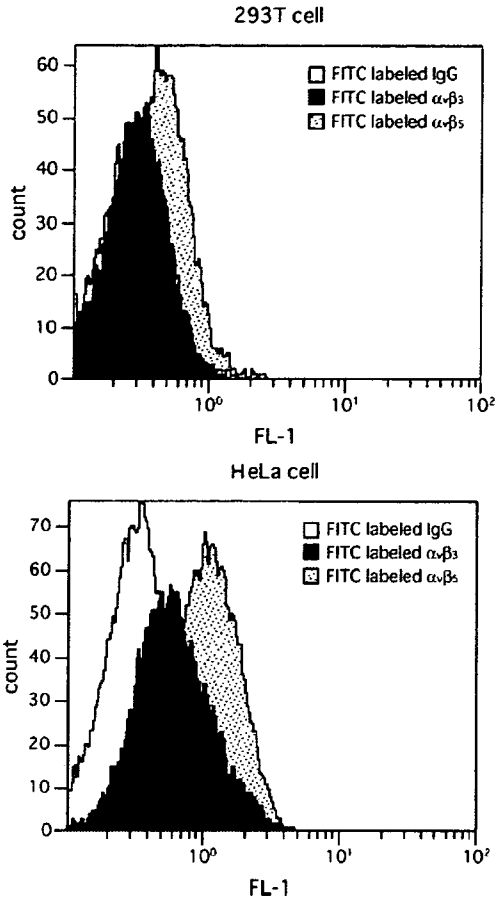

Figure 4. Flow cytometric analysis of integrin expression on 293T cells (left) and HeLa cells (right).

Transfection. *In vitro* TE of polyplex micelles was evaluated for 293T cells and HeLa cells at varying transfection times (Figure 5). PEG−PLys/pDNA micelles without the peptide ligand and RGDS−PEG−PLys/pDNA micelles with a linear RGD peptide ligand were used as controls. RGD peptide is the adhesion motif of extracellular matrix proteins for the various types of integrins (*20*, *21*). The linear RGD peptide showed a binding affinity for $\alpha_v\beta_3$ integrin approximately 1/1000 of that of the cyclic RGD peptide (*22*). In the transfection experiment using 293T cells, there were no differences in the TE of the three types of micelles at any of the transfection times. This finding is consistent with the observation that 293T cells showed low integrin expression (Figure 4). On the other hand, in the transfection experiment using HeLa cells, c(RGDfK)−PEG−PLys micelles achieved a significantly higher TE than PEG−PLys and RGDS−PEG−PLys micelles. It is reasonable to assume that HeLa cells might efficiently recognize c(RGDfK) ligands on the micelle through $\alpha_v\beta_3$ and $\alpha_v\beta_5$ integrins expressed on their surface. Nevertheless, the TE of linear RGD peptide-conjugated micelles toward HeLa cells was comparable to that of the micelles without any ligand, suggesting that the binding affinity of the linear RGD peptide for the integrins might be insufficient to increase the TE.

Analysis of Cellular Uptake of Polyplex Micelles. The cellular uptake of the micelles into the HeLa cells was evaluated by a flow cytometer using fluorescein-labeled pDNA-incorporated micelles with varying incubation times (Figure 6). The amount of the uptake was always higher for c(RGDfK)−PEG−

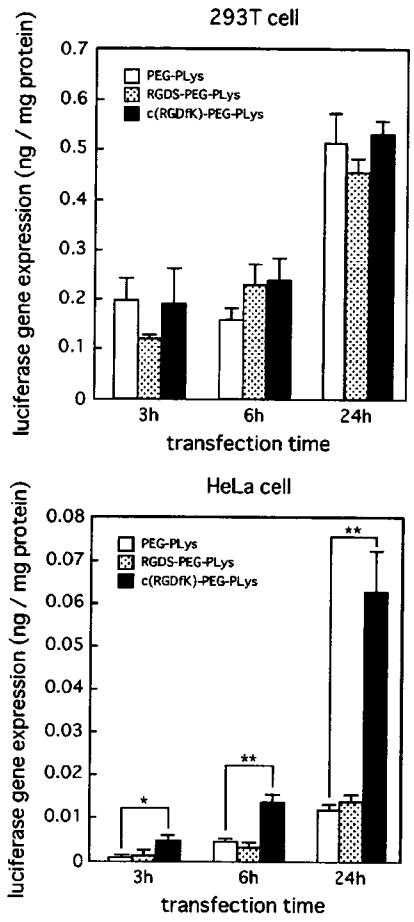

Figure 5. Effect of cell lines and transfection time on gene expression. 293T cells (left) and HeLa cells (right) were transfected with PEG–PLys, RGDS–PEG–PLys, and c(RGDfK)–PEG–PLys micelles prepared at N/P = 2 in a medium containing 10% serum. The data are the mean ± SEM, $n = 4$. $P^* < 0.05$ and $P^{**} < 0.01$.

PLys micelles than for PEG–PLys micelles at each incubation time, which suggests that the specific interaction of the cyclic RGD peptide with integrin receptors on the HeLa cells contributed to the uptake amount. In 24 h incubation, the amount of c(RGDfK)–PEG–PLys micelles that were taken up was 1.6 times the amount of PEG–PLys micelles taken up (Figure 6B). Nevertheless, c(RGDfK)–PEG–PLys micelles revealed an even higher TE of approximately 5 times that of the PEG–PLys micelles (Figure 5). This implied that other factors besides the enhanced uptake might also play a role in the enhanced TE observed for HeLa cells challenged with c(RGDfK)–PEG–PLys micelles.

Intracellular Distribution of Polyplex Micelles. The intracellular distribution of polyplex micelles was investigated by CLSM using Cy5-labeled pDNA-incorporated micelles with 3 h incubation, and typical images from this investigation are shown in Figure 7. A large fraction of the Cy5-labeled pDNA was still distributed near the cell membrane for the cells challenged with PEG–PLys polyplex micelles (Figure 7A). Alternatively, an appreciable accumulation of the Cy5-labeled pDNA in the perinuclear regions was observed for the cells challenged with c(RGDfK)–PEG–PLys polyplex micelles (Figure 7B). Further detailed observation using LysoTracker, which labels acidic late endosome and lysosome, revealed that the majority of c(RGDfK)–PEG–PLys polyplex micelles were localized in the acidic compartments as indicated by the yellow color in the merged fluorescence image of the Cy5-labeled pDNA (red) and LysoTracker (green), yet a fraction that did not co-localize with LysoTracker was also observed, suggesting that at least some of the polyplex micelles in the perinuclear regions may be located in a site other than the lysosomes.

DISCUSSION

There are many barriers to achieve effective transfection using nonviral gene vectors. Stability in the bloodstream and specific cellular uptake by the target tissues and organs are major obstacles, especially for *in vivo* gene delivery. Polyplex micelles with PEG as a hydrophilic shell layer have been shown to achieve an increased retention time in the bloodstream (*5*), and they are promising candidates for vectors that can be used for *in vivo* gene delivery. Also, the introduction of targetable ligands onto polyplex micelles has been reported, and some of the ligand-installed polyplex micelles have been demonstrated to be effective both in *in vivo* as well as *in vitro* transfection (*6–8*). The ligands on polyplex micelles may facilitate their internalization into the target cells, thus increasing the TE. A number of studies have aimed to find suitable ligands for this purpose (*23*), and cyclic RGD peptides have been highlighted as one of the promising candidates (*7*). Cyclic RGD peptides are well-known to selectively recognize $\alpha_v\beta_3$ and $\alpha_v\beta_5$ integrins, which are overexpressed in angiogenic endothelial cells in tumors. Therefore, a targetable gene delivery system equipped with a cyclic RGD peptide as the ligand may be useful for antiangiogenic therapy for tumors (*24*, *25*).

In this study, to construct polyplex micelles showing integrin-mediated gene transfection, the novel synthetic route of a block copolymer with a c(RGDfK) peptide ligand was exploited as summarized in Scheme 1. The acetal group may be converted to an aldehyde group under acidic conditions. Thus, the TFA group was selected to protect the primary amino group of the lysine units, because it can be removed under basic conditions without any conversion of acetal groups to aldehyde groups. The introduction of peptide ligands was then carried out under mild acidic conditions with good yields in a one-pot reaction involving the conversion of acetal groups to aldehyde groups and the subsequent conjugation of the ligand through the formation of a thiazolidine ring as seen in Scheme 1. In this way, various peptide ligands having a cysteine end group (Cys-peptide) may be readily introduced into the block copolymer. Moreover, this type of conjugation reaction between aldehyde and Cys-peptide occurs selectively even in the presence of primary amines, because the formation of a Schiff base between a primary amine and an aldehyde is reversible and thus sensitive to pH, while the thiazolidine ring formation between the N-terminal cysteine and aldehyde is an irreversible reaction. This reaction is available for the introduction of various ligands into the block copolymer, not only peptides but also other ligand molecules possessing an N-terminal cysteine.

Indeed, as confirmed by the NMR spectra shown in Figure 2, the c(RGDfK) peptide, which can peculiarly recognize $\alpha_v\beta_3$ and $\alpha_v\beta_5$ integrins, was successfully introduced into the PEG terminus of the PEG–PLys block copolymer as a targetable ligand molecule. The c(RGDfK)–PEG–PLys/pDNA micelle achieved a higher TE compared to nontargetable PEG–PLys and RGDS–PEG–PLys micelles against HeLa cells, which express an appreciable amount of $\alpha_v\beta_3$ and $\alpha_v\beta_5$ integrins. In contrast, there was no difference in TE among these three types of polyplex micelles against 293T cells, which show a limited expression of $\alpha_v\beta_5$ integrin, but no expression of $\alpha_v\beta_3$ integrin. This result is consistent with a previous report which found that the $\alpha_v\beta_3$ integrin has an approximately 10-times higher binding affinity for the cyclic RGD peptide than the $\alpha_v\beta_5$ integrin (*26*), which suggests that the $\alpha_v\beta_3$ integrin may be involved in an increased TE against HeLa cells by means of the c(RGDfK)–PEG–PLys/pDNA micelle. Flow cytometric analysis (Figure

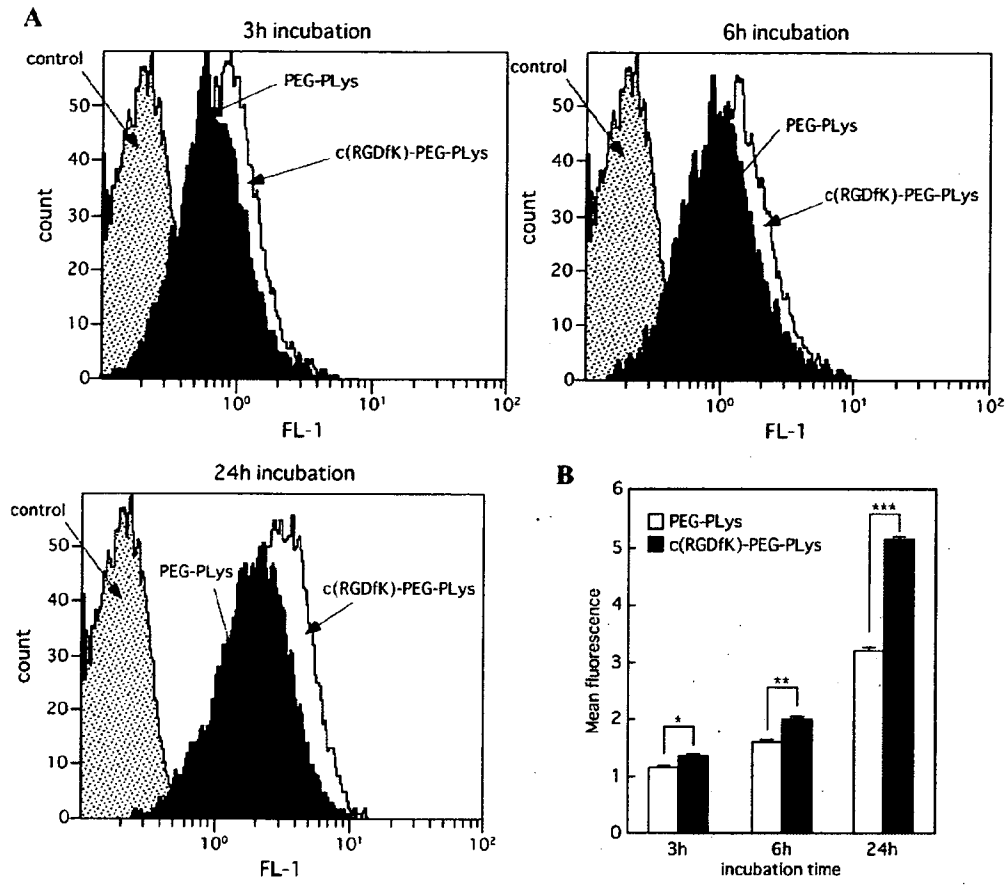

Figure 6. Cellular uptake of polyplex micelles. PEG−PLys and c(RGDfK)−PEG−PLys micelles loaded with fluorescein-labeled pDNA were applied to HeLa cells with varying incubation times. (A) Flow cytometric histogram profiles of time-dependent change in fluorescence intensity. (B) Mean fluorescence intensity at each incubation time. The data are the mean ± SEM, $n = 3$. $P^* < 0.05$, $P^{**} < 0.01$, and $P^{***} < 0.001$.

6) also suggests that the enhanced uptake of the c(RGDfK)−PEG−PLys/pDNA micelle might contribute to an increased TE against HeLa cells. Interestingly, the difference in the uptake ratio against the HeLa cells between the c(RGDfK) micelle and the ligand-free micelle became more significant with increased incubation time as seen in Figure 6. Integrin receptors are known to recycle to the plasma membrane through an endocytic cycle every 15−40 min (*27*). Consequently, this fast recycle of integrins might contribute to the facilitated uptake of the c(RGDfK) micelle into the HeLa cells in comparison with the ligand-free micelle. Nevertheless, as can be seen from Figures 5 and 6B, the uptake ratio is not simply correlated in a time-dependent manner with the TE. The ligand effect appeared to be more significant in the TE than in the uptake ratio, particularly after a prolonged time period such as 24 h. This result led us to assume that the c(RGDfK) ligand may also affect intracellular trafficking of the polyplex micelles. Indeed, a CLSM observation of HeLa cells challenged with polyplex micelles revealed a substantial difference in intracellular distribution between the PEG−PLys and c(RGDfK)−PEG−PLys micelles (Figure 7). In the cells challenged with the PEG−PLys polyplex micelle, a majority of pDNA was still distributed near the cell membrane, whereas in the same time frame of 3 h the cells with the c(RGDfK)−PEG−PLys polyplex micelle showed an appreciable accumulation of pDNA in the perinuclear region. It is noteworthy that a definite fraction of pDNA (colored red) in the perinuclear region did not co-localize with LysoTracker (colored green), suggesting that this fraction may be located in a compartment other than the acidic late endosome and lysosome. The $\alpha_v\beta_3$ integrin receptors have been reported to pass rapidly through the early endosomes, arriving at the perinuclear compartments approximately 30 min after internalization (*28*). Recent reports have shown an active transport pathway for a nonviral gene delivery system (*29*, *30*), in which microtubule-associated motor proteins have contributed to a rapid perinuclear accumulation of the polyplex within minutes after transfection. Also, recent studies have revealed that polyplexes in the perinuclear region but not in the acidic compartments significantly contribute to the effective transfection (*31*, *32*). These phenomena are consistent with our observation of a partial accumulation of the c(RGDfK)−PEG−PLys micelle in the perinuclear sites but outside of the acidic compartments, suggesting that the enhancement of the TE of the polyplex micelle by the introduction of cyclic RGD peptide ligands might be due not only to the enhanced uptake but also to the change in the intracellular trafficking route directed to the nucleus. It is likely that the micelle fraction distributed in nonacidic compartments near the nucleus may efficiently internalize into the nucleus when the cells are in the dividing phase, thus contributing to the increase in the transfection. Although the effective transport of the PLys-based polyplex micelles from the isolated compartment into the cytoplasm remains an issue because of inefficiency in the PLys function of facilitating the endosome-escaping step, the conjugation of c(RGDfK) ligands onto the polyplex micelle surface has great potential to improve the TE through modulated intracellular trafficking.

In conclusion, a successful synthetic route involving block copolymers conjugated with peptidyl ligands through thiazolidine ring formation was developed in this study. Cyclic RGD peptide-conjugated polyplex micelles showed an increased TE against HeLa cells possessing $\alpha_v\beta_3$ and $\alpha_v\beta_5$ integrins because